processes

MDPI

Article

Demulsification of Water-in-Oil Emulsion with Carbon Quantum Dot (CQD)-Enhanced Demulsifier

Jhon F. Gallego [1], Oscar E. Medina [1,*], Jose A. Tengono [2], Camilo Mazo [2], Andres F. Maya [2], Cristina Caro [2], Farid B. Cortés [1,*] and Camilo A. Franco [1,*]

[1] Grupo de Investigación en Fenómenos de Superficie—Michael Polanyi, Departamento de Procesos y Energía, Facultad de Minas, Universidad Nacional de Colombia, Sede Medellín, Medellín 050034, Colombia; jfgallegoa@unal.edu.co

[2] Jefatura de Gestión de Activos, HOCOL S.A., Bogotá 110111, Colombia; jose.tengono@hocol.com.co (J.A.T.); camilo.mazo@hocol.com.co (C.M.); andres.maya@hocol.com.co (A.F.M.); cristina.caro@hcl.com.co (C.C.)

* Correspondence: oemedinae@unal.edu.co (O.E.M.); fbcortes@unal.edu.co (F.B.C.); caafrancoar@unal.edu.co (C.A.F.)

Abstract: This study aims to optimize the demulsification performance of a carbon quantum dot (CQD)-enhanced chemical demulsifier in industrial emulsions under thermal, mechanical, and thermomechanical effects. Experiments were conducted to assess treatments like organic treatment (OT), zeta potential modifier aqueous solution (ZPMAS), and acid treatment (9.25 wt.% HCl) at varying dosages, along with CQD–chemical mixtures optimized through a simplex-centroid mixture design (SCMD) to minimize basic sediment and water (BSW). Under the thermomechanical scenario, a system with 500 mg·L^{-1} CQDs and OT achieves 0.5% BSW and a droplet size of 63 nm, while an SCMD-optimized system (500 mg·L^{-1} CQDs + 380 mg·L^{-1} OT + 120 mg·L^{-1} ZPMAS) achieves 0% BSW and larger droplets (>70 nm). CQDs enhance demulsifiers by destabilizing water-in-oil (W/O) Pickering emulsions, leveraging their nanometric size, high surface area, thermal conductivity, and amphiphilicity, thanks to their hydrophobic core and surface hydrophilic groups (-OH, NH_2, -COOH). This research enhances the understanding of demulsification by employing green demulsifiers based on CQDs and provides a promising cost-efficient solution for breaking stable emulsions in the petroleum industry. It minimizes the use of complex and expensive active ingredients, achieving BSW values below 0.5%, the standard required for crude oil transport and sale, while also reducing separation equipment operation times, and improving overall process efficiency.

Keywords: carbon quantum dots; chemical demulsifier; green demulsifier; simplex-centroid mixture design; statistical analysis; water-in-oil emulsion

check for updates

Academic Editor: Lin He

Received: 14 January 2025
Revised: 11 February 2025
Accepted: 12 February 2025
Published: 18 February 2025

Citation: Gallego, J.F.; Medina, O.E.; Tengono, J.A.; Mazo, C.; Maya, A.F.; Caro, C.; Cortés, F.B.; Franco, C.A. Demulsification of Water-in-Oil Emulsion with Carbon Quantum Dot (CQD)-Enhanced Demulsifier. *Processes* **2025**, *13*, 575. https://doi.org/10.3390/pr13020575

Copyright: © 2025 by the authors. Licensee MDPI, Basel, Switzerland. This article is an open access article distributed under the terms and conditions of the Creative Commons Attribution (CC BY) license (https://creativecommons.org/licenses/by/4.0/).

1. Introduction

Crude oil extraction is often accompanied by brine production, particularly in mature reservoirs where chemical-enhanced oil recovery methods rely on large volumes of water [1]. This water emulsifies into crude oil during production, complicating transportation [2,3]. As a result, crude oil typically contains 1–60% water [4]. Although water and oil are immiscible, stable water-in-oil (W/O) emulsions can form due to interfacial active compounds (e.g., asphaltenes, resins, and fine solids) and the shear stress exerted during pipeline transport [5]. Compared to crude oil, these emulsions are more voluminous and viscous, increasing energy consumption, pipeline corrosion, and scaling, ultimately reducing pipeline efficiency [6]. Additionally, high water content lowers the commercial

value of crude oil [6]. The extreme viscosity and adhesive nature of W/O emulsions hinder transportation and pose challenges in refining, including catalyst poisoning. Therefore, efficient water separation before transport and refining is essential for operational and economic efficiency [7,8].

Emulsion stability is influenced by multiple factors, including temperature, pH, water droplet size, viscosity, oil-to-brine ratio, interfacial tension, and phase density differences [9]. Stability increases with smaller water droplets, higher continuous-phase viscosity, lower interfacial tension, and reduced density contrast between phases [10–12]. Natural surfactants and co-surfactants, such as resins and asphaltenes, further affect emulsion stability by adsorbing at the oil–water interface, reducing zeta potential and interfacial tension due to their hydrophilic functional groups, thereby forming interfacial films [13–16]. Resins generate weaker films with thinner asphaltene layers, resulting in less stable emulsions, while asphaltenes form strong, thick films that enhance stability [17,18]. Additionally, asphaltenes and resins can interact synergistically to further stabilize emulsions [19,20]. The primary mechanism for crude oil emulsion stabilization is the formation of a viscoelastic film through asphaltene aggregation and cross-linking [17,21,22]. Adsorbed polymers, surfactants, and particles create elastic interfacial films that inhibit water droplet coalescence [17,23]. Solids also contribute to the stability of water-in-oil (W/O) emulsions. When stabilized by solids such as hydrophobic silica, iron oxide, crystalline waxes, clays, corrosion products, and mineral scales, they form W/O Pickering emulsions [24,25]. Stability increases with higher solid concentrations and smaller particle sizes [24,26]. Finely divided solids, such as clays, stabilize emulsions through two main mechanisms: (i) solid adsorption at the oil–water interface, forming a protective film around water droplets; and (ii) particle–particle interactions creating a three-dimensional network in the oil phase that surrounds the dispersed water droplets [26]. Due to their high stability, even with large droplet sizes, W/O Pickering emulsions pose significant challenges in the oil and gas industry by complicating water and solid separation from crude oil [14–16].

Numerous studies have explored water separation techniques to address emulsion stability challenges [27,28]. These efforts have focused on various treatment methods, including filtration [29,30], electrostatic separation [31,32], hydrocyclones [33], centrifugation [34], biological and chemical demulsification [35–37], flotation [34,38], membrane separation [39,40], catalytic desalination [41,42], and ultrasonic and microwave demulsification [43,44], as well as adsorption using porous materials such as aerogels [45] and sponges [46]. While these methods offer certain advantages, they often fail to fully meet the demands of downstream industries. Therefore, the development of more efficient and adaptable separation techniques remains crucial.

Chemical demulsification is widely used as a complementary method to thermal and mechanical treatments, helping to accelerate the demulsification process and reduce the operating time of conventional equipment such as ovens and centrifuges [27]. Chemical demulsifiers function by adsorbing at the oil–water interface, weakening the interfacial film in water-in-oil (W/O) emulsions. They typically consist of solvents, coagulants, and surface-active additives (surfactants) [17]. Coagulants destabilize solids by neutralizing their anionic surface charge, allowing particle aggregation [47]. Solvents, including xylene, toluene, short-chain alcohols, and benzene, serve as carriers in demulsifier formulations and aid in solubilizing natural emulsifiers such as asphaltenes and resins, promoting water droplet coalescence [17,48,49]. Surfactants are essential for reducing interfacial film strength, with hydrophilic demulsifiers being particularly effective in W/O emulsions dominated by asphaltenes and lipophilic surfactants [17,50]. Demulsifiers with a hydrophile–lipophile balance (HLB) above 8 are preferred for breaking W/O emulsions, as those with HLB values between 3 and 8 tend to act as emulsifiers instead [51]. Despite extensive research

and product development aimed at destabilizing emulsions, the widespread application of chemical demulsifiers remains limited due to high costs associated with their elevated concentration requirements and the presence of complex chemical additives such as flocculants, coagulants, and surfactants [1].

Nanotechnology offers a promising approach to enhancing water separation efficiency by improving demulsification performance and reducing the need for complex chemical additives such as flocculants, coagulants, and surfactants [1]. Various studies have explored the potential of nanoparticles as substitutes or enhancers for conventional chemical demulsification methods [2,3]. The three primary types of nanoparticles investigated for oil–water emulsion treatment are silica, magnetic nanoparticles, and modified graphene oxide (GO) [25,52–56]. Fang-Hui et al. [4] demonstrated that dispersing SiO_2 nanoparticles in a polyether demulsifier increased the emulsion's dehydration rate by approximately 20% at a 1:10 mass ratio of SiO_2 to polyether. Similarly, Wang et al. [57] developed an in situ polyether demulsifier with SiO_2 nanoparticles, achieving a significant reduction in demulsification time (shortened by ~30 min) at the same nanoparticle-to-polyether ratio. Peng et al. [58] investigated a non-magnetic demulsifier, achieving up to 90% water separation efficiency, which was attributed to the interfacial activity of the nanomagnetic demulsifier. Magnetic nanoparticles (MNPs) have also demonstrated high demulsification efficiencies. Wang et al. [59] designed core–shell MNPs by stabilizing Fe_3O_4 nanoparticles with oleic acid (OA) and grafting them with cetrimonium bromide (CTAB), achieving a 98.1% demulsification efficiency. Mao et al. [60] developed core–shell polymer nanoparticles (PBM@PDM) that promoted water droplet coalescence by replacing asphaltenes at the water–oil interface, resulting in an 85% dehydration ratio at 21 °C with 800 $mg \cdot L^{-1}$ of PBM@PDM. Lu et al. [61] synthesized alkyl/amino-siloxane-modified magnetic nanoparticles (Fe_3O_4@SiO_2), reporting a 95% demulsification efficiency for both oil-in-water (O/W) and water-in-oil (W/O) emulsions due to their amphiphilic and cationic nature. Graphene oxide (GO)-based nanomaterials have also shown remarkable demulsification performance. Liu et al. [62] attributed the exceptional efficiency (>99.9%) of amphiphilic GO nanosheets to their strong interaction with asphaltenes at optimal GO concentrations. Chen et al. [63] explored hyperbranched polyamidoamine-graphene oxide magnetic nanoparticles (GO-MNPs), achieving a 99.1% demulsification efficiency at 20 $mg \cdot L^{-1}$, pH 6, and 40 °C. Even after seven reuse cycles, efficiency remained high at 97%. However, despite their effectiveness, the large-scale production of GO-based nanomaterials remains challenging due to high costs and low synthesis efficiency [64].

Despite significant advancements in nanoparticle synthesis for W/O demulsification, developing a cost-effective and eco-friendly methodology for producing nanoparticles with tunable properties remains a key research challenge. Most nanomaterial-based demulsifiers are not economically viable due to the complexity of functionalizing nanoparticles or fabricating core–shell and graphene oxide (GO)-based materials [4,57–65]. Carbon quantum dots (CQDs) offer a promising alternative. These zero-dimensional, carbon-based nanoparticles (<10 nm) share similarities with GO but are significantly more cost-efficient [66]. CQDs are biocompatible, non-toxic, and photoluminescent, and have been widely applied in fields such as drug delivery, optoelectronics, photocatalysis, ion detection, supercapacitors, fuel cells, bioimaging, and photovoltaics [67–79]. Their amphiphilic nature arises from hydrophilic functional groups (hydroxyl, carbonyl, carboxyl) on the surface, while their hydrophobic carbon core is rich in C=C bonds [67,80]. This unique chemistry enables CQDs to interact with both crude oil and saltwater at the interface, suggesting potential demulsification capabilities. However, despite their promising properties, no studies have yet explored the application of CQDs in W/O demulsification, highlighting an important research opportunity.

This study aimed to optimize the effectiveness of a novel chemical demulsifier enhanced with carbon quantum dots (CQDs) to address the challenges of water-in-oil (W/O) emulsions. For the first time, CQDs were incorporated into a chemical demulsifier to enhance demulsification performance, offering a groundbreaking approach to overcoming the limitations of traditional methods in the oil and gas industry. To achieve this, three conventional chemical demulsifiers and CQDs were evaluated under thermal, mechanical, and thermomechanical separation methods, allowing for a detailed analysis of thermal and mechanical effects on W/O emulsion demulsification. The optimal concentration for each chemical demulsifier was determined, and the three most effective treatments were subsequently combined using a simplex-centroid mixture design. This approach enabled the optimization of demulsifier concentrations, maximizing efficiency in emulsion breaking under thermomechanical separation.

The incorporation of carbon quantum dots (CQDs) represents a significant advancement in demulsification technology, offering a promising solution to improve separation processes in the oil and gas industry. This innovative approach addresses the limitations of conventional chemical demulsifiers, particularly their high costs and reliance on complex chemical formulations [1]. By reducing the need for expensive active ingredients, CQDs contribute to the development of more eco-friendly and cost-efficient demulsifiers. Moreover, compared to most nanomaterial-based demulsifiers, which often involve intricate and costly synthesis processes [4,57–65], CQDs offer a simpler, more economical alternative while maintaining high demulsification efficiency.

2. Materials and Methods

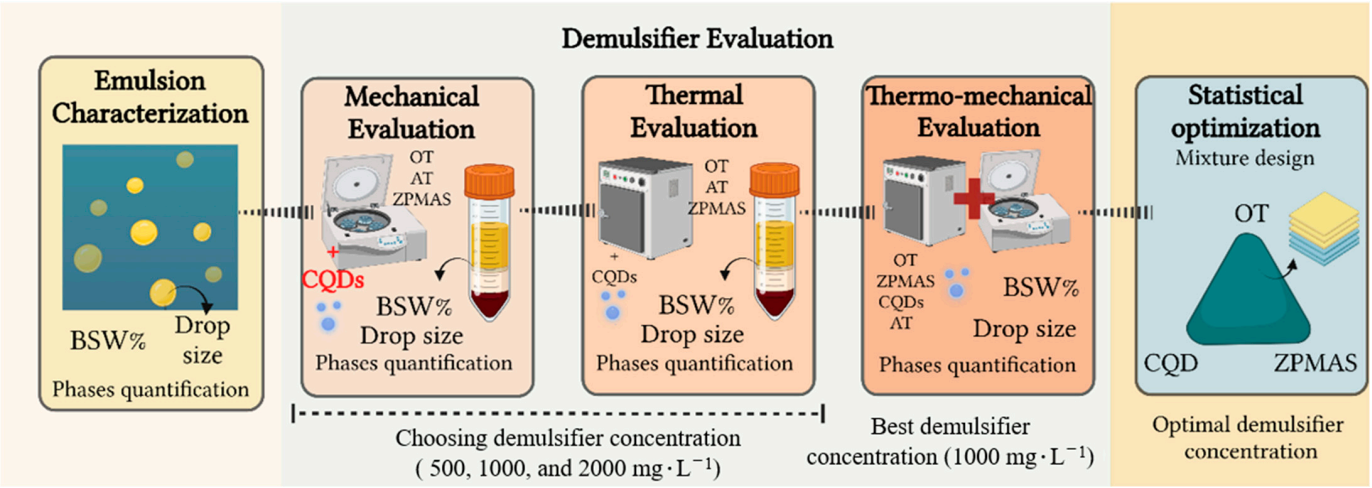
2.1. Materials

A water-in-oil emulsion with basic sediment and water (BSW) of 50% was used for the experiments and obtained from a Colombian oil field in the Meta department. A 37 wt.% hydrochloric acid purchased from PanReac (AppliChem, Maryland Heights, MO, USA) was diluted to obtain a 9.25 wt.% solution, which was employed as a demulsifier (acid treatment—AT) due to its solids' coagulant capacity due to its low pH [11]. The zeta potential modifier aqueous solution (ZPMAS) was mainly composed of inorganic salts and surfactant compounds, which were purchased from Petroraza S.A.S (Sabaneta, Colombia) and evaluated because of its capacity to promote solid coagulation [47]. Additionally, an organic treatment (OT), which is a mixture of alcohols, diesel, and xylene, was provided by Petroraza S.A.S (Sabaneta, Colombia) and was also evaluated because of its solvent nature and capacity to dissolve natural emulsifiers such as resins and asphaltenes due to its aromatic compounds, avoiding the presence of the natural emulsifiers in the water/oil interphase [48,49]. Carbon quantum dots (CQDs) were synthesized following the protocol of a previous work [67] and evaluated as demulsifiers because of their surface-active properties that might promote water droplet coalescence by locating at the O/W interface [67]. Moreover, CQDs might alter the wettability of solids in the emulsion [81–83] and increase the heat transfer efficiency by increasing the convective heat transfer coefficient and the thermal conductivity [84]. Toluene, heptane, and carbon disulfide (CS_2) (all provided by Sigma Aldrich, Burlington, MA, USA) were used to wash the deposited solids.

2.2. Methods

Scheme 1 illustrates the comprehensive experimental roadmap employed in this study to characterize the emulsions and assess the efficacy of various demulsifier treatments. Initially, the emulsions were characterized to establish a baseline for the study. This characterization includes measuring the basic sediment and water (BSW) content, determining the size distribution of water droplets within the emulsions, and categorizing the emulsion

phases into four distinct categories to provide a detailed understanding of their composition and structure.



Scheme 1. Experimental roadmap used in this study for emulsion characterization and evaluation of demulsifier treatment efficacy.

Demulsifier evaluation was conducted in three stages. The mechanical evaluation was performed in the first stage. Three conventional demulsifier treatments and carbon quantum dots (CQDs) were considered, each mixed with the emulsions, and the effectiveness of the demulsification process was measured. Thermal treatment was evaluated in the subsequent stage. The same demulsifiers used in the first stage were tested. The emulsions were thermally treated to determine the impact of heat, in conjunction with the CQDs and conventional demulsifier treatments, on demulsification. Based on the mechanical and thermal results, the demulsifier concentration was selected for further study in a combined thermomechanical stage. This stage involved applying thermal treatment followed by mechanical centrifugation to the emulsions treated with the selected demulsifiers and measuring the resulting demulsification efficiency to understand the synergistic effects of heat and mechanical action. Finally, to optimize the demulsification process under thermomechanical evaluation, the three best chemical demulsifiers were selected to be mixed in various proportions based on a statistical mixture design. This stage aimed to identify the most effective combination of treatments and optimize the proportions to achieve maximum demulsification efficiency.

2.2.1. Characterization of the Chemical Demulsifiers

The chemical demulsifiers were characterized using Fourier transform infrared spectroscopy (FTIR), surface tension, density, conductivity, pH, and hidrophile–lipohile balance (HLB) number. An FTIR test was carried out to corroborate the presence of functional groups and to identify the chemical nature of the chemical demulsifiers. This test was carried out using an IRAffinity-1S infrared spectrophotometer (Shimadzu, Kyoto, Japan). The measurement was performed at room temperature in the wavenumber range of 4000–650 cm^{-1} with a resolution of 2 cm^{-1}. The surface tensions of the treatments were measured using an Attension Sigma 702ET force tensiometer (Biolin Scientific, Stockholm, Sweden). The density of the treatments was obtained using an Attention Sigma 702ET force tensiometer (Biolin Scientific, Stockholm, Sweden). Conductivity was measured using an Orion Star™ A212 Conductivity Benchtop Meter (Thermo Scientific™, Waltham, MA, USA), while pH was determined using a digital pH meter TEC-7/1-MP (TECNAL, Piracicaba, Brazil). The HLB number was calculated for the chemical demulsifiers and

optimum CQD-enhanced demulsifier as described by Chun et al. [85]. In this procedure, the HLB number is calculated using Equation (1). For this purpose, the interfacial tension of the aqueous solution with the corresponding demulsifier at 0.1% overlayered with toluene in a beaker of 50 mL was measured using an Attension Sigma 702ET force tensiometer (Biolin Scientific, Stockholm, Sweden). Three measurements were taken and averaged, with Zuidema-Waters correction applied to each measurement.

$$\mathrm{HLB} = -\frac{(\gamma - 45.8)}{2.36} \quad (1)$$

2.2.2. Emulsion Characterization

The emulsion was initially characterized by determining the basic sediment and water (BSW). It was calculated using a standard test method, ASTM D96, to determine the water and sediments in crude oil by centrifugation. In the experimental procedure, a 100 mL pear-shaped graduated centrifuge tube was employed. To initiate the process, 50 mL of toluene was introduced into a centrifuge tube, and then 50 mL of the sample was added. The mixture in the centrifuge tube was vigorously manually stirred for 2 min. Subsequently, the centrifuge tube was stirred within the centrifuge at 3000 rpm for 10 min. The final step involved determining the basic sediment and water (BSW) content by distinguishing the percentages corresponding to water and sediments. Furthermore, at this step, the percentage of the phases comprising basic sediment and water was distinguished and read for each phase (Phase 2–4). The emulsion was characterized based on the water droplet radius distribution, which was assessed using optical microscopy (OM). The sample was examined under optic microscopy using a Motic BA310 microscope (Motic, Stockholm, Sweden) with the objective 10x/0.25 (WD 17.4 mm). Subsequently, micrographs of the droplets present in the samples were captured. Percentile 50 of the droplet size distribution (D_{50}) was determined to indicate the representative water droplet size and as a sign of emulsion stability because smaller water droplet sizes indicate a high emulsion stability, making an emulsion more difficult to break [10–12]. A photographic record of the phases obtained from the emulsion after the BSW test (stirring at 3000 rpm for 10 min with 50% v/v toluene) is shown in Figure S1 in the Supporting Material Information. Furthermore, the emulsion phases were characterized to understand the nature of the emulsions.

Separation of Phases of the W/O Emulsion

To characterize the different phases of the emulsion, they were first separated, as presented in this section. To facilitate the complete separation of the phases within the emulsion, a mechanical separation process was employed by centrifugation at 4500 rpm for 6 h using a Hermle Z 306 Universal Centrifuge (Labnet, Edison, NJ, USA). The outcome revealed four distinct phases: (i) Phase 1: crude oil; (ii) Phase 2: crude oil/water interphase; (iii) Phase 3: solids as a deposit; and (iv) Phase 4: water phase located between Phases 2 and 3. The deposited solids were treated with subsequent solvent washings with toluene, heptane, and carbon disulfide (CS_2), as described in Figure 1, to remove the major part of the organic compounds in the sample. Toluene was initially used to dissolve asphaltenes and aromatic compounds. Heptane, a non-polar solvent was then introduced to dissolve waxes and saturates while promoting asphaltene precipitation. Finally, carbon disulfide (CS_2) was employed for its superior solvent capacity, effectively dissolving both polar and non-polar compounds, including resins, asphaltenes, and waxes [86]. For this purpose, 125 mg of the sample was added to 25 mL of solvent at 300 rpm for 12 h with each solvent. Photographic records of phase 2 (crude oil/water interphase) and phase 3 (deposit solids) before and after washing with organic solvents are shown in Figure S2 in the Supporting

Material Information. It is worth mentioning that these phases (Phases 1–4) were only considered to characterize the emulsion.

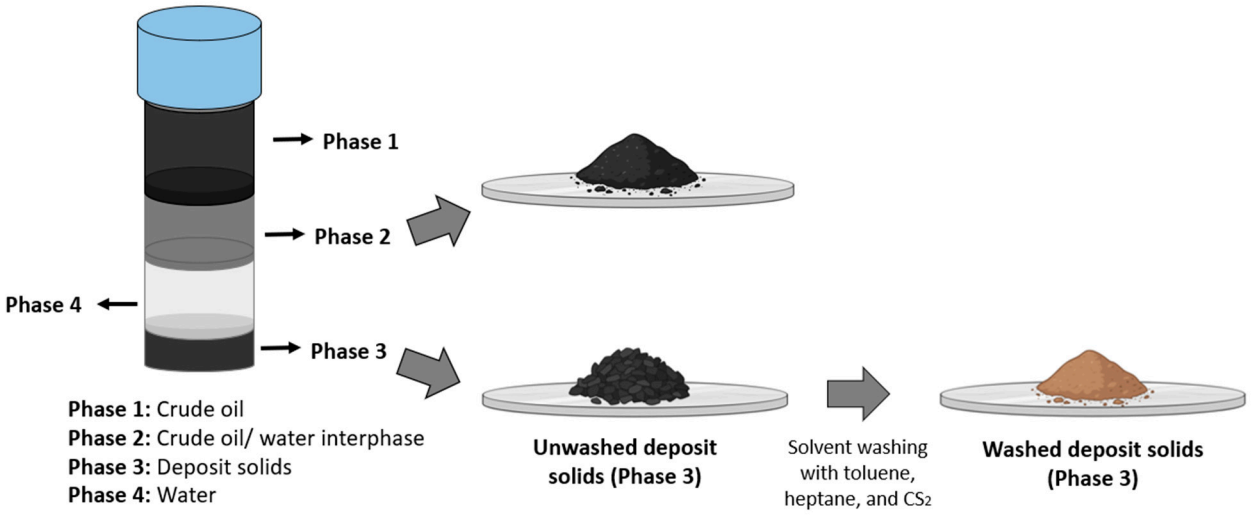


Figure 1. Scheme of emulsion phase separation. Four emulsion phases were identified: Phase 1, crude oil; Phase 2, crude oil/water interphase; Phase 3, deposited solids; and Phase 4, water. The deposited solids (Phase 3) were treated with successive solvent washings with toluene, heptane, and CS_2.

Characterization of the Crude Oil (Phase 1)

The saturate, aromatic, resin, and asphaltene (SARA) content of crude oil (Phase 1) obtained in Section "Separation of phases of the W/O emulsion" was determined following the ASTM D6560 standard method [87] in conjunction with Iatroscan procedure IP 469 [88] using a TLC-FID/FPD Iatroscan MK6 (Iatron Labs Inc., Tokyo, Japan) [89]. The dynamic viscosity and density were determined using an SVM 3000 Stabinger Viscosimeter (Anton Paar, Graz, Austria), according to the ASTM D7042 standard method [90]. The specific gravity was obtained from the crude oil density. The API gravity was determined from specific gravity at 15.6 °C according to the API gravity scale developed by the American Petroleum Institute. The Colloidal Instability Index (CII) is the ratio of the sum of saturates and asphaltenes to the sum of resins and aromatics [91,92]. This ratio can be used to estimate the stability of asphaltenes in crude oil [93]. The CII was calculated as described in Equation (2).

$$\text{CII} = \frac{\text{saturates} + \text{asphaltenes}}{\text{aromatics} + \text{resins}} \quad (2)$$

Characterization of the Emulsion Phases Through Dissolution and Thermogravimetric Analysis

The four phases obtained from the emulsion following the procedure described in Section "Separation of phases of the W/O emulsion" were characterized by thermogravimetric analysis (TGA) to discretize the fraction of organic and inorganic solids in each phase. The thermogravimetric analysis was conducted using a thermogravimetric balance (TGA Q50, Inc., New Castle, DE, USA) at ambient pressure, achieving equilibrium at 30 °C and a subsequent temperature ramp of 20 °C min^{-1} up to 800 °C. This process involved a balanced purge flow of N_2 at 10 mL min^{-1} and a sample purge flow of N_2 at 90 mL min^{-1}. The crude oil phase, crude oil/water interphase, and deposit solid phase were further characterized through dissolution tests. Dissolution tests were performed by immersing the samples of each phase in 25 mL of solvent at a concentration of 5000 mg·L^{-1}. Four solvents were used: water, HCl 1M, toluene, and heptane. Finally, the washed deposit solids were characterized by Fourier transform infrared spectroscopy (FTIR, 450 to 4500 cm^{-1})

analysis using an IRAffinity-1S spectrophotometer (Shimadzu, Kyoto, Japan) to determine the nature of the inorganic solids. The washed deposit solids were also analyzed by X-ray diffraction (XRD) using a Bruker Advance D-8 X-ray diffractometer (Billerica, MA, USA) with a Cu Kα radiation source (λ = 0.154 nm) operated at 40 kV and 40 mA. The XRD data were collected between 10° and 90° (2θ) with a resolution of 0.02° (2θ).

2.2.3. Evaluation of Demulsifiers Under Thermal, Mechanical, and Thermomechanical Separation Methods

Three scenarios were evaluated to evaluate the performance of chemical demulsifiers under mechanical (centrifugation), thermal (temperature), and thermomechanical (centrifugation followed by temperature) separation methods. (i) Scenario of mechanical separation (Figure 2a): 100 mL of the emulsion was added to a beaker of 100 mL. The chemical demulsifier (AT, OT, CQDs, or ZPMAS) was then added to the beaker with the emulsion at 0, 500, 1000, and 2000 mg·L^{-1}. The mixture was stirred at 50 rpm using a digital ULTRA-TURRAX homogenizer (Yamato Scientific Co., Ltd., Tokyo, Japan) for 10 min. The sample was then centrifuged at 4500 rpm for 20 min. (ii) Scenario of thermal separation (Figure 2b): 100 mL of the emulsion was added to a beaker of 100 mL. Subsequently, a chemical demulsifier (AT, OT, CQDs, or ZPMAS) at concentrations of 0, 500, 1000, and 2000 mg·L^{-1} was added to the emulsion. Subsequently, each mixture was stirred at 50 rpm for 10 min using a digital ULTRA-TURRAX homogenizer. Later, each sample was placed in an oven at 67.2 °C for 24 h. Temperature was selected according to its operational value in the field of interest. (iii) Thermomechanical separation (Figure 2c): 100 mL of the emulsion was mixed with the corresponding chemical demulsifier (CQDs, AT, OT, or ZPMAS) at the best demulsifier concentration (1000 mg·L^{-1}) based on previous scenarios. The mixture was stirred at 50 rpm for 10 min using a digital ULTRA-TURRAX homogenizer and centrifuged at 4500 rpm for 15 min. Subsequently, a micrograph of the sample was obtained for the posterior droplet size distribution analysis. Then, the sample was placed in an oven at 67.2 °C for 6 h, following the droplet size of the emulsion every hour.

The resulting oil phase of each system after thermal, mechanical, and thermomechanical separation scenarios was extracted with a syringe and characterized by determining the representative water droplet size (D_{50}) under optic microscopy using a Motic BA310 microscope (Motic, Stockholm, Sweden) with the objective 10X/0.25 (WD 17.4 mm). Then, 50 mL of the extracted oil phase was used for BSW measurement according to the ASTM D96 standard method. In this procedure, 50 mL of toluene was added to a centrifuge tube, followed by the addition of 50 mL of the oil phase and vigorous manual stirring for 2 min. The tube was then centrifuged for 10 min at 3000 rpm. Finally, BSW was determined by distinguishing basic water and sediment percentages. Furthermore, the percentages of water, O/W interphase, and solids were also characterized as phases comprising basic water and sediments.

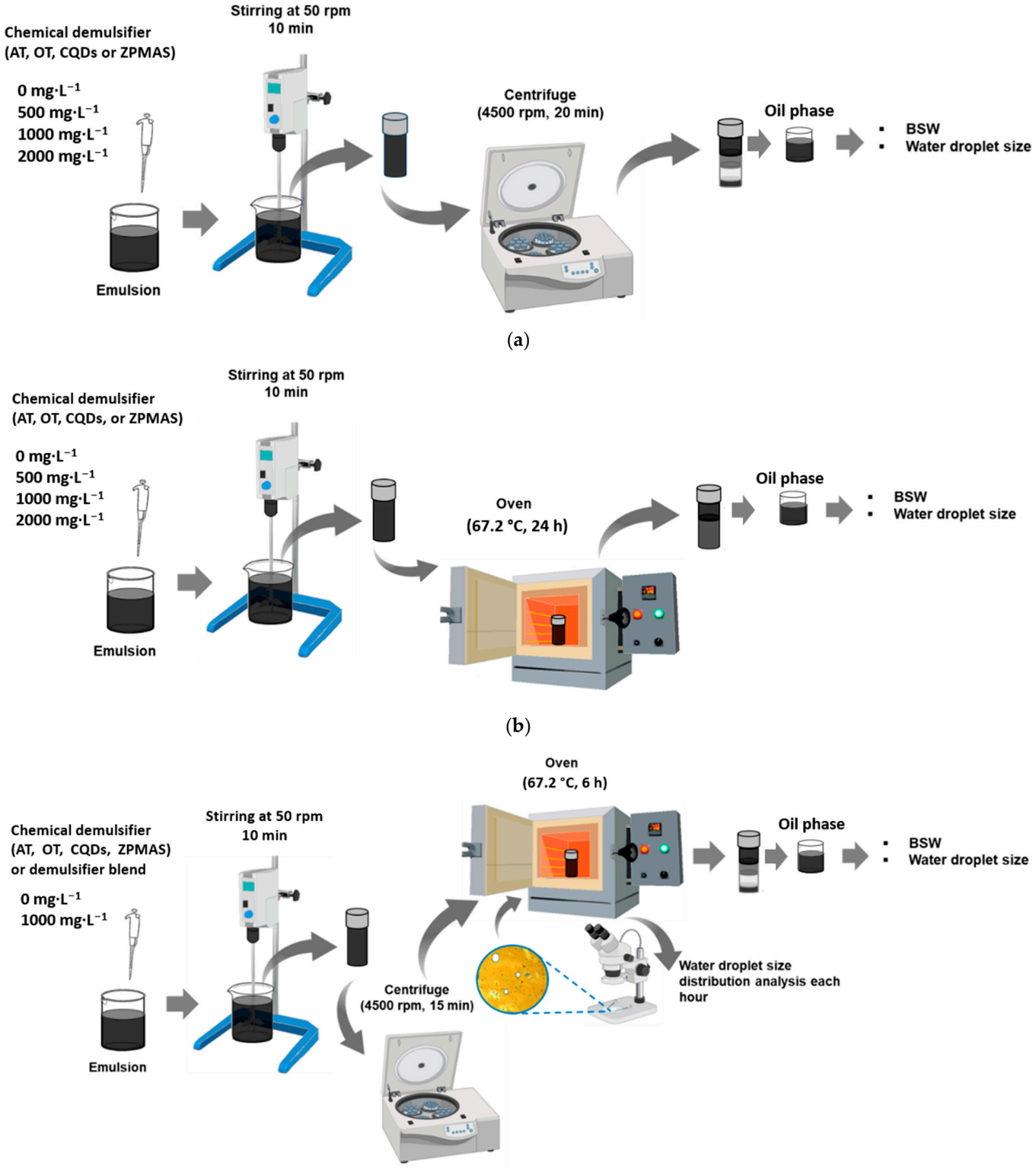


Figure 2. Scheme of the experimental procedure for evaluating chemical demulsifiers under: (**a**) mechanical, (**b**) thermal, and (**c**) thermomechanical separation scenarios. Four phases were distinguished in the experiments of the mechanical and thermomechanical separation scenarios.

2.2.4. Water and Sediment Remotion Efficiency Under Thermal, Mechanical, and Thermomechanical Separation Methods

To determine the performance of demulsifiers in the demulsification process for each scenario of separation, under (i) thermal, (ii) mechanical, and (iii) thermomechanical separation, a water and sediment removal efficiency ($W\&S_{remotion}$) was proposed and calculated as follows in Equation (3):

$$W\&S_{remotion}(\%) = 100 \cdot \left(\frac{BSW\%_{emulsion} - BSW\%_{demulsifier}}{BSW\%_{emulsion}} \right) \quad (3)$$

where $BSW\%_{emulsion}$ is the BSW% value of the original emulsion (50%), and $BSW\%_{demulsifier}$ is the BSW% value of the system in the presence of the demulsifier at the desired concentration.

2.3. Experimental Mixture Design for Thermomechanical Separation

An experimental design was employed to determine the optimal CQD (carbon quantum dots) blend with the two most effective conventional chemical demulsifiers, OT and ZPMAS. The objective was to minimize the basic sediment and water (BSW) content in the crude oil phase under the scenario of thermomechanical separation. The experiment employed a simplex-centroid mixture design (SCMD) using the STATGRAPHICS Centurion XVI software from StartPoint Technologies Inc., Addison, TX, USA. This design variation involved adjusting the mass fractions of CQDs, OT, and ZPMAS. The SCMD is a technique used to forecast the response of a chosen parameter based on the variability of a controlled variable. Notably, the proportion of each component must follow specific restrictions [94]:

$$\sum_{i=1}^{n} x_1 + x_2 + x_3 + \ldots + x_n = 1 \qquad ; \; x_i \geq 0 \quad (4)$$

The "n" parameter corresponds to the number of components varying in the mixture. In this case, n = 3 represents three components: x_1 for the ZPMAS, x_2 for the CQDs, and x_3 for the OT. Therefore, the limits for each compound were as follows:

$$0 \leq ZPMAS \leq 1 \quad (5)$$

$$0 \leq CQDs \leq 1 \quad (6)$$

$$0 \leq OT \leq 1 \quad (7)$$

The maximum and minimum dosages of each component were then determined. Furthermore, other specific points were considered, including pairs of components with a mass ratio of 0.5, for each component. Another point of interest was the scenario in which all the three mixture components had an equal mass ratio of 0.333, as shown in Figure 3. A special cubic regression was used to model BSW. The regression model equation is as follows:

$$BSW = \beta_1 \cdot x_1 + \beta_2 \cdot x_2 + \beta_3 \cdot x_3 + \beta_{12} \cdot x_1 \cdot x_2 + \beta_{13} \cdot x_1 \cdot x_3 + \beta_{123} \cdot x_1 \cdot x_2 \cdot x_3 \quad (8)$$

where β_i, β_{ij}, and β_{ijk} are the coefficients of the linear terms, binary mixtures of non-additive components, and ternary mixtures of non-additive components, respectively.

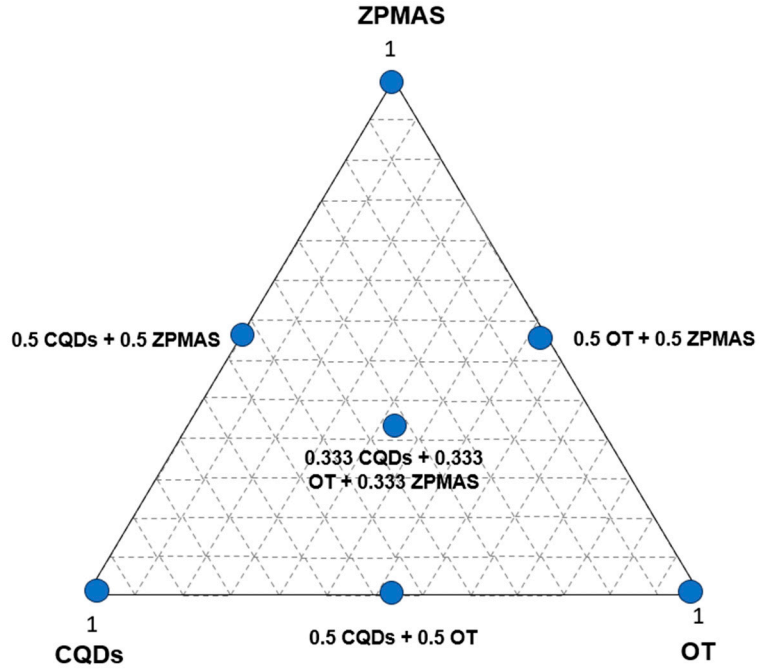


Figure 3. Experimental points of the simplex-centroid mixture design (SCMD) with the proportions of each component (ZPMAS, CQDs, and OT) in mass fraction under the thermomechanical separation scenario.

3. Results and Discussion

3.1. Fluid Characterization

3.1.1. Characterization of Chemical Demulsifiers

The basic physicochemical characteristics of the chemical demulsifiers, such as density, surface tension, conductivity, and pH, are presented in Table 1. The demulsifier with the highest density was the CQDs, whereas the one with the lowest density was the OT, owing to its organic nature. The pH increased in the order AT < OT < ZPMAS < CQDs, whereas the conductivity and surface tension increased in the order OT < ZPMAS < CQDs < AT. The HLB number ranged between 5 and 13 for the four demulsifiers and increased in the order of CQDs < ZPMAS < AT < OT. OT has an HLB number of 12.36, which might be due to the high hydrophilicity caused by alcohol groups [95].

Table 1. Basic physicochemical characterization of chemical demulsifiers used in the formulation.

Demulsifier	Density [kg·L^{-1}]	Surface Tension [mN·m^{-1}]	Conductivity [μS·cm^{-1}]	pH	HLB
AT	1.0459	69.1 ± 0.7	446 × 10^3 ± 3 × 10^3	0.15 ± 0.01	7.51
ZPMAS	1.0826	34.1 ± 0.9	1719 ± 10	5.22 ± 0.01	5.90
OT	0.8629	28.0 ± 0.1	0.26 ± 0.01	3.95 ± 0.01	12.36
CQDs	1.3624	58.1 ± 1.3	3134 ± 17	6.03 ± 0.01	5.69

Figure S3 of the Supporting Information shows the functional groups of demulsifiers identified by Fourier transform infrared spectroscopy (FTIR) analysis. Figure S3a shows a characteristic band of O-H tension between 3550 and 3584 cm^{-1} for the three conventional demulsifiers. A band corresponding to the C-H tension was observed for OT and ZPMAS [96]. Moreover, AT and ZPMAS presented a peak at 1630 cm^{-1}, indicating the presence of water in their composition and confirming their water-based nature [97]. Finally, OT presented an absorption band around 1060 cm^{-1} corresponding to C-O tension, a characteristic group of a primary alcohol compound, which corroborates the presence of

alcohol in its composition [96]. For the CQDs, as shown in Figure S3b, distinctive bands at 3350–3310 cm^{-1} (N-H stretching) and 1550–1500 cm^{-1} (N-O stretching) confirm the presence of nitrogen in the CQDs [67]. Two absorption bands corresponding to O-H tension were observed at 3700–3550 cm^{-1} and 3100–2000 cm^{-1}. Furthermore, two characteristic bands of C=O tension appeared at 1760 and 1710 cm^{-1}, respectively. Finally, the absorption bands at 980–960 cm^{-1} and 730–665 cm^{-1} (C=C flexion) indicated the presence of alkenes [96].

3.1.2. Emulsion Characterization

An image of the sample obtained after the BSW test is shown in Figure S1. The BSW of the emulsion was approximately 50%. As shown in Table 2, the BSW was discretized in Phase 2: water–oil interphase (26%); Phase 3: deposit solids (12%); and Phase 4: water (12%). The emulsion had an average water droplet radius (D_{50}) of 0.40 µm, which, according to the literature, is indicative of a highly stable emulsion [10–12,98].

Table 2. Basic characteristics of the emulsion.

Property		Value
%BSW	Phase 2: Crude oil/water interphase	26
	Phase 3: Deposit solids	12
	Phase 4: Water	12
	Total	50
Average water droplet radius—D_{50} (µm)		0.4

The deposited solids (Phase 3) were washed with toluene, heptane, and CS_2 as detailed in Section "Separation of phases of the W/O emulsion". The percentage of weight loss with toluene and heptane regarding the initial sample mass was nearly 37%, while after CS_2 solvent washing, the weight loss was approximately 47% of the initial sample mass, which means that 10% of the sample was additionally dissolved when using CS_2.

Basic Characterization of the Crude Oil (Phase 1)

The crude oil (phase 1) in the emulsion presented an API gravity of 24.2°, characteristic of intermedium oils. The basic characteristics of the crude oil, such as saturated, aromatic, resin, and asphaltene (SARA) contents, are presented in Table 3. The Colloidal Instability Index (CII) calculated from the SARA analysis indicates that asphaltenes are unstable in the crude oil phase [27,93], which can promote asphaltene migration to the W/O interphase and stabilize the emulsion because of their aromatic and polycyclic aromatic groups [93,99].

Table 3. Basic characterization of the emulsion's crude oil (Phase 1) after emulsion phase separation.

Property		Crude Oil (Phase 1)
%BSW		<0.1%
Specific gravity at 15.6 °C		0.9
API gravity at 15.6 °C		24.2
Dynamic viscosity (cP) at 15.6 °C		46.4
SARA Analysis	Saturates (%)	49.9
	Aromatics (%)	12.3
	Resins (%)	34.1
	Asphaltenes (%)	3.7
	CII	1.15

Characterization of Emulsion Phases Through Dissolution and Thermogravimetric Analysis

The collected samples of the three phases (including Phase 1: crude oil; Phase 2: water/crude oil interphase; and Phase 3: solids (unwashed and washed with toluene, heptane, and CS_2)) were characterized by thermogravimetric analysis to determine their organic and inorganic composition and the boiling point for the assurance of not losing mass at 67.2 °C. The results are shown in Figure 4. Crude oil TGA is shown in panel a. Initially, a small weight loss associated with the evaporation of the remaining free water present in the crude oil was observed. Light crude oil often contains water, which can be observed as a decrease in its weight at lower temperatures. As the temperature increases, volatile components with lower boiling points evaporate (probably butanes and isobutanes). The main decomposition of crude oil occurs in this region. Various hydrocarbons within crude oil start to break down into lighter fragments, leading to gradual weight loss. The residue left behind at higher temperatures represents the more stable and higher-boiling components of crude oil, such as heavier hydrocarbons commonly associated with asphaltenes. The sample from Phase 2 (panel b) exhibited slight differences from the crude oil sample. The intensity of the first peak decreased, suggesting a lower release of light hydrocarbons [100]. The peaks at higher temperatures were like those for asphaltenes. The main difference is that the remaining sample was heated to 800 °C, which is related to the inorganic content (3 wt.%). The solids collected from the emulsion depicted a TGA profile (panel c) with 37.7 wt. % of inorganic compounds, and after being washed with hydrocarbons and CS_2, it increased up to 73.9 wt.% (panel d).

To describe the chemical nature of Phases 2 and 3, their dissolution in different fluids, including water, HCl at 1M, *n*-heptane, and toluene, was evaluated. Here, three systems were analyzed: the water/crude oil interphase and the solids before and after washing with hydrocarbons and CS_2. The results are shown in Figure 5. The sample obtained from Phase 2 (water/crude oil interphase) showed 59% and 78% dissolution in heptane and toluene, respectively, which confirms the presence of asphaltenes since there is a higher dissolution of Phase 2 as asphaltenes are soluble in toluene and insoluble in heptane [101,102]. The dissolution of solids (Phase 3) increased in the order of water < HCl < heptane < toluene. However, after washing, the trend changed, resulting in higher dissolution in water and HCl owing to the destruction of the organic compounds. This result is congruent with the TGA results presented previously. Note that the unwashed solids from Phase 3 were poorly soluble in water because of the presence of organic compounds on the surface of the inorganic solids, confirming the hydrophobic nature of these solids in the emulsion. These hydrophobic solids promote the stabilization of the emulsion by tending to locate in the continuous phase (oil) surrounding the dispersed water droplets, thereby enhancing the emulsion stability [24,26,103].

Finally, the FTIR spectra of the solids washed with hydrocarbons, and CS_2 are shown in Figure 6a. Some inorganic functional groups were identified by analyzing the mean peaks in the graph. Si-OH was detected at 3690 cm^{-1} [104]; Si-O-Si, between 1000 and 1100 cm^{-1} [105]; Si-O-Ca, at 930 cm^{-1} [105]; $CaCO_3$, between 1200 and 1500 cm^{-1} [105]; and FeO, at 560 cm^{-1} [106,107]. Some organic functional groups such as CH_3, CH_2, C-H, and C=O were observed at 2924, 2870, 1450, and 1680 cm^{-1}, respectively [96]. Finally, an OH group was observed at 3400 cm^{-1} [96].

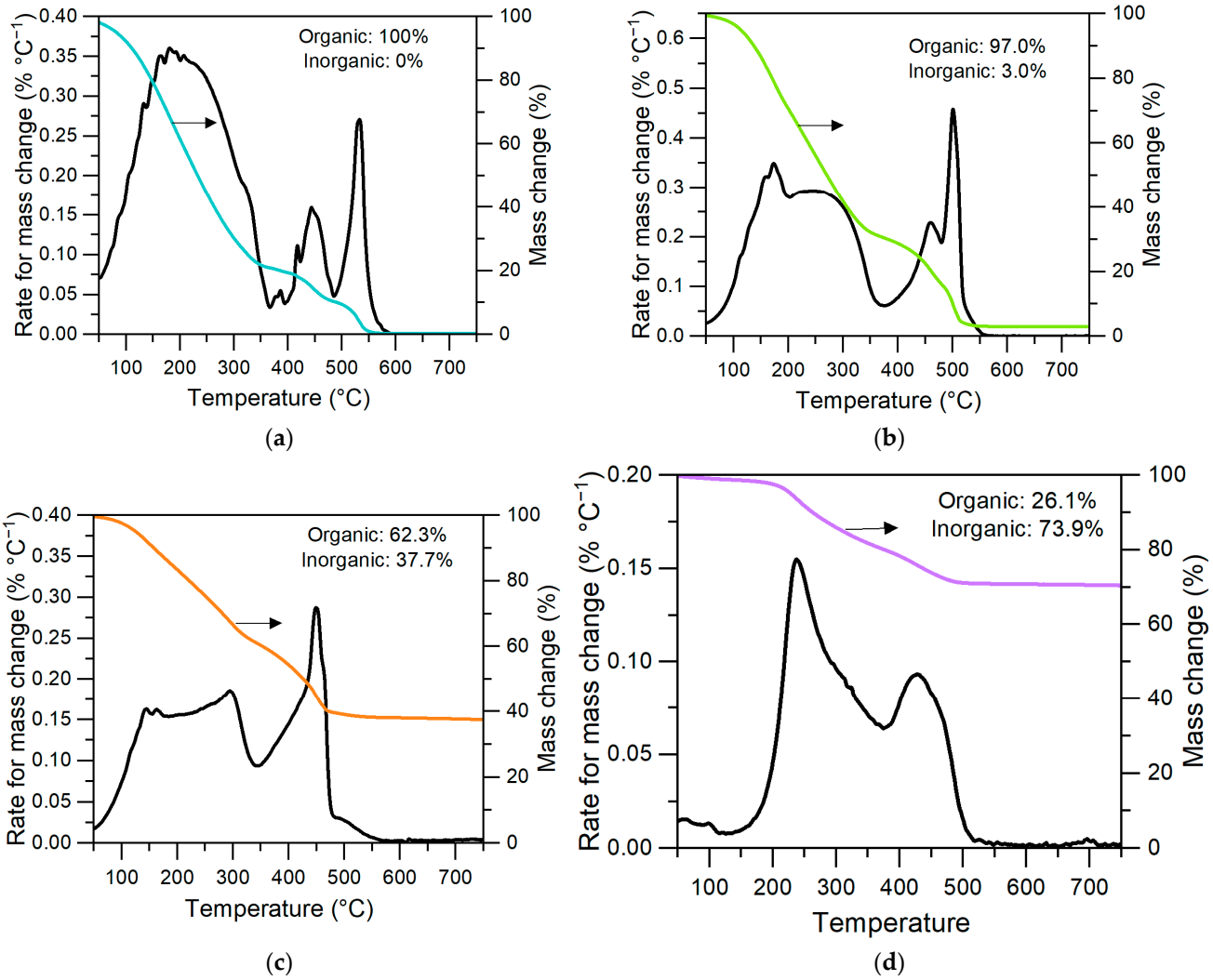


Figure 4. Thermogravimetric analysis of (**a**) Phase 1: crude oil; (**b**) Phase 2: water/crude oil interphase; (**c**) unwashed deposit solids (Phase 3); and (**d**) deposit solids (Phase 3) washed successively with toluene, heptane, and CS_2.

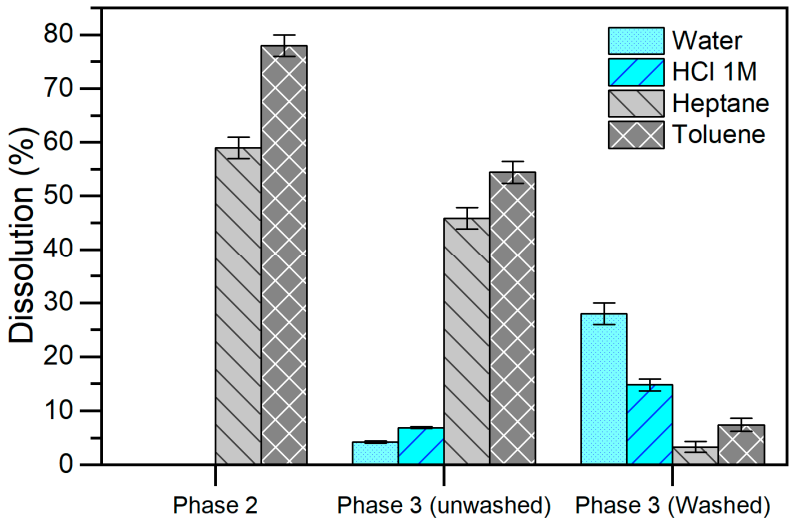


Figure 5. Dissolution results in water, HCl (1 M), heptane, and toluene for Phase 2: the water/crude oil interphase and Phase 3: the unwashed and washed deposit solids.

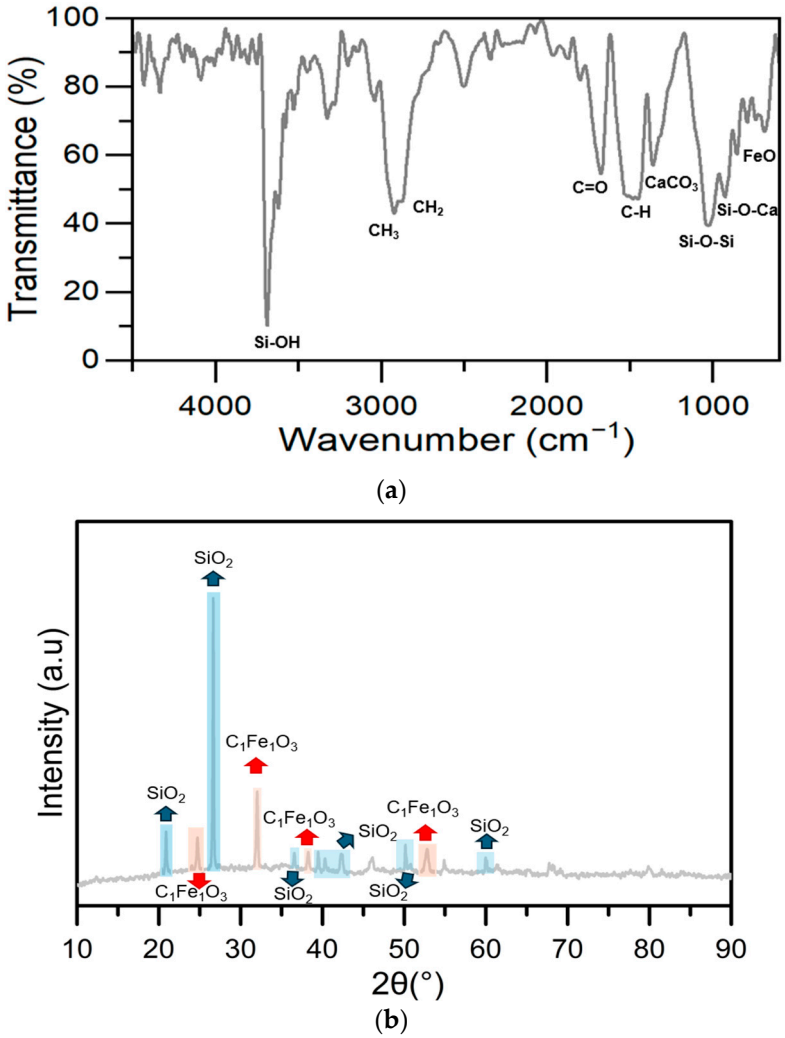


Figure 6. (**a**) FTIR spectrum and (**b**) XRD spectrum of solids after being washed with toluene, heptane, and CS_2.

The XRD patterns are shown in Figure 6b. The washed deposit solids exhibit diffraction peaks characteristic of SiO_2/quartz (ref: 98-008-3849) at 20° (010), 26° (011), 36° (110), 40° (111), 42° (020), 45° (201), 50° (003), and 59° (121). Also, siderite ($C_1Fe_1O_3$) characteristic peaks were observed at 24°, 32°, 38°, and 52°, corresponding to the crystal facets: (012), (104), (110), and (116), respectively.

3.2. Demulsification of Water-in-Oil Emulsion

3.2.1. Mechanical Separation Scenario

Figure 7 shows the oil phase's average droplet radius and BSW% under the mechanical separation scenario for the chemical treatment (CQDs, ZPMAS, AT, and OT) and the base emulsion with no demulsifier addition. The treatments were applied at different concentrations (500, 1000, and 2000 mg·L^{-1}), and the water droplet radius and BSW were measured. The base emulsion with no demulsifier addition under mechanical evaluation presented an average droplet radius (D_{50}) of 12.5 µm and a BSW% of ~14%. The base emulsion exhibited a removal efficiency of approximately 72%. Note that the lowest droplet size was obtained for the base emulsion with no demulsifier treatment (0 mg·L^{-1}). At each concentration level, droplet size followed a consistent trend across treatments. The droplet size increased in the following order: ZPMAS < AT < OT < CQDs. The chemical composition of the demulsifier and its interactions with crude oil components influence

emulsion stability and droplet size [10]. Therefore, interactions might be more favorable with OT compared to the other conventional treatments (AT and ZPMAS), improving the coalescence of droplets and leading to larger droplet sizes, which can be mainly related to the aromatic compounds of diesel and xylene in OT, which can favor the solubility of resins and asphaltenes, avoiding their presence in the water/oil interphase and their surfactant-like effect due to their polar and non-polar groups [108]. Furthermore, OT can promote the reduction of asphaltene and resin aggregates owing to its solvent nature, which reduces the interfacial film strength [49,109]. However, CQD systems presented a larger droplet size, mainly because of their high surface hydrophilicity, favoring dispersed water droplet coalescence [110]. CQDs may destabilize the emulsion by locating at the O/W interface owing to their hydrophilic nature, adsorbing at the interfacial film competitively against asphaltenes and resins, which promotes the reduction of the asphaltenes and resins at the interfacial film [17,111]. Moreover, CQDs promote wettability alteration in fine solids that strengthen the interfacial film. Hence, adding CQDs to the W/O emulsion leads to a wettability alteration that stabilizes fine solids from oil-wet to water-wet [81,82], which displaces solids from the interface and therefore reduces the strength of the interfacial film.

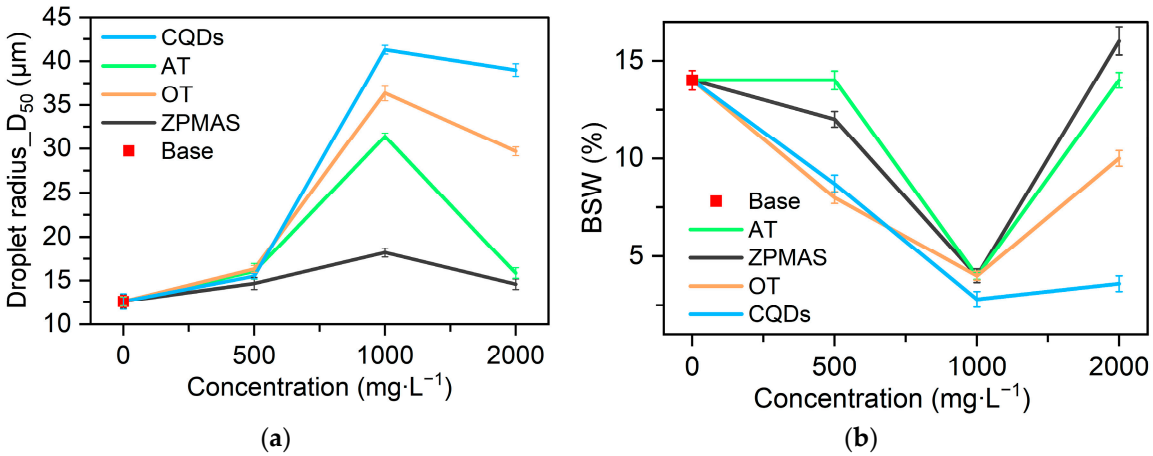


Figure 7. (**a**) Average droplet radius (D_{50}) and (**b**) BSW% of the oil phase depending on the treatment concentration for the conventional treatments OT, ZPMAS, and AT under the mechanical separation scenario. Base emulsion with no demulsifier treatment addition is also shown at a concentration of 0 mg·L^{-1}.

Interestingly, there was a very interesting behavior at 1000 mg·L^{-1} where the droplet size was larger for all treatments than the adjacent concentrations (500 and 2000 mg·L^{-1}). This behavior suggests that the droplet size does not follow a linear trend at a concentration of 1000 mg·L^{-1} for all three treatments. The concentration of the demulsifiers (CQDs, ZPMAS, AT, and OT) at 1000 mg·L^{-1} may be within the range where their behavior changes. This could lead to less effective stabilization of the emulsion droplets, resulting in larger droplets. The system may reach a saturation point or become overloaded at 1000 mg·L^{-1}, where the emulsifier can no longer effectively stabilize the droplets, resulting in increased coalescence and larger droplet sizes, as reported in the literature [112].

The information from the BSW (basic sediment and water) of the oil phase is shown in panel b. Below 1000 mg·L^{-1}, the BSW increases in the order OT < CQDs < ZPMAS < AT with remotion efficiency values for OT, CQDs, ZPMAS, and AT of 84%, 83%, 76%, and 72%, respectively. This suggests that at concentrations lower than 1000 mg·L^{-1}, the treatments had a differential impact on the BSW, with OT and CQDs presenting the lowest BSW values, followed by ZPMAS and AT. A noteworthy observation is that at 1000 mg·L^{-1}, the BSW is lower for all treatments compared to concentrations below and above 1000 mg·L^{-1}. At a

treatment concentration of 1000 mg·L^{-1}, the BSW values obtained with ZPMAS, AT, and OT were approximately 4%, which represents a removal efficiency of 92%, much higher than that of the base emulsion (72%), whereas CQDs presented a BSW of 3% with a removal efficiency of 94%. This indicates that there might be a concentration threshold effect at 1000 mg·L^{-1}, leading to a consistent reduction in BSW for all treatments. At 2000 mg·L^{-1}, the BSW order changed to CQDs< OT < AT < ZPMAS with removal efficiencies of 93%, 80%, 72%, and 68% for CQDs, OT, AT, and ZPMAS, respectively.

In considering both graphs (Figure 7a,b), there seems to be an inverse correlation between droplet size and BSW. When the droplet sizes are smaller, the BSW tends to be higher and vice versa. A favorable concentration for both properties was found at 1000 mg·L^{-1}, where droplet sizes were higher for all treatments than adjacent concentrations, the BSW was lower for all treatments, and the values were very similar. Therefore, the higher droplet sizes and lower BSW found at a concentration of 1000 mg·L^{-1} indicate a higher degree of demulsification and better performance of the treatments, as reported in the literature [10].

Figure 8 shows the percentage of water and water/crude oil interphase in the oil phase at varying treatment concentrations (CQDs, OT, ZPMAS, and AT). At 500 mg·L^{-1} (panel a), a clear trend was observed, with the water/crude oil interphase decreasing in the order AT (14%) > ZPMAS (11%) CQDs (9%) > OT (8%). This suggests that OT and CQDs at 500 mg·L^{-1} were the most effective chemical demulsifiers for reducing the water/crude oil interphase. Also, the water content of all treatments remained consistently below 1%, indicating effective treatment in minimizing the presence of the emulsion.

At 1000 mg·L^{-1}, all treatments showed a significant reduction in water/crude oil interphase, dropping below 5%. This implies that, specifically at this concentration, the treatments uniformly resulted in higher water and oil separation. Like the water/crude oil interphase, the water content for all treatments remained below 1%, demonstrating the effectiveness of the treatments in controlling emulsion formation. However, CQDs presented the lowest water/crude oil interphase content with a value below 3%. At the highest treatment concentration of 2000 mg·L^{-1}, the water/oil interphase increased in the order CQDs < OT < AT < ZPMAS. ZPMAS. Notably, it stands out by showing the highest increase, approaching 16%, which is slightly higher than that of base emulsion. This trend indicates that the CQDs demonstrate superior performance in reducing the water content and water/crude oil interphase across the entire treatment concentration range. In particular, CQDs at concentrations of 1000 mg·L^{-1} and 2000 mg·L^{-1} had a higher impact on reducing the stability of the emulsions.

The CQDs consistently appeared to be the most effective in reducing the water/crude oil interphase at all concentrations. Also, water content remains controlled, staying below 1% for most concentrations and treatments. The concentration of the treatments played a pivotal role in modifying the emulsion characteristics since lower BSW values represented by the water and water/oil interphase were observed at 1000 mg·L^{-1} regardless of the treatment. The results indicate that each treatment has an optimal concentration range near 1000 mg·L^{-1} for maximum effectiveness, highlighting the importance of precise concentration selection in emulsion treatment processes. Excessive demulsifier addition can reduce emulsion breakdown efficiency, as reported in the literature [112–114], due to the formation of a viscoelastic film on the water droplet surface, which stabilizes the dispersed phase and isolates the demulsifying molecules [113]. This trend in which there is an optimal concentration of demulsifier to promote emulsion breaking has been obtained in previous experimental studies [112,114]. For instance, Mohyaldinn et al. evaluated the performance of polyvinylpyrrolidone (PVP) as a demulsifier using a bottle test (i.e., heating at 60 °C followed by stirring). The authors found that among the range of demulsifier

concentrations evaluated (i.e., 10 to 80 mg·L^{-1}), the optimum concentration with the highest water separation was 60 mg·L^{-1} [114].

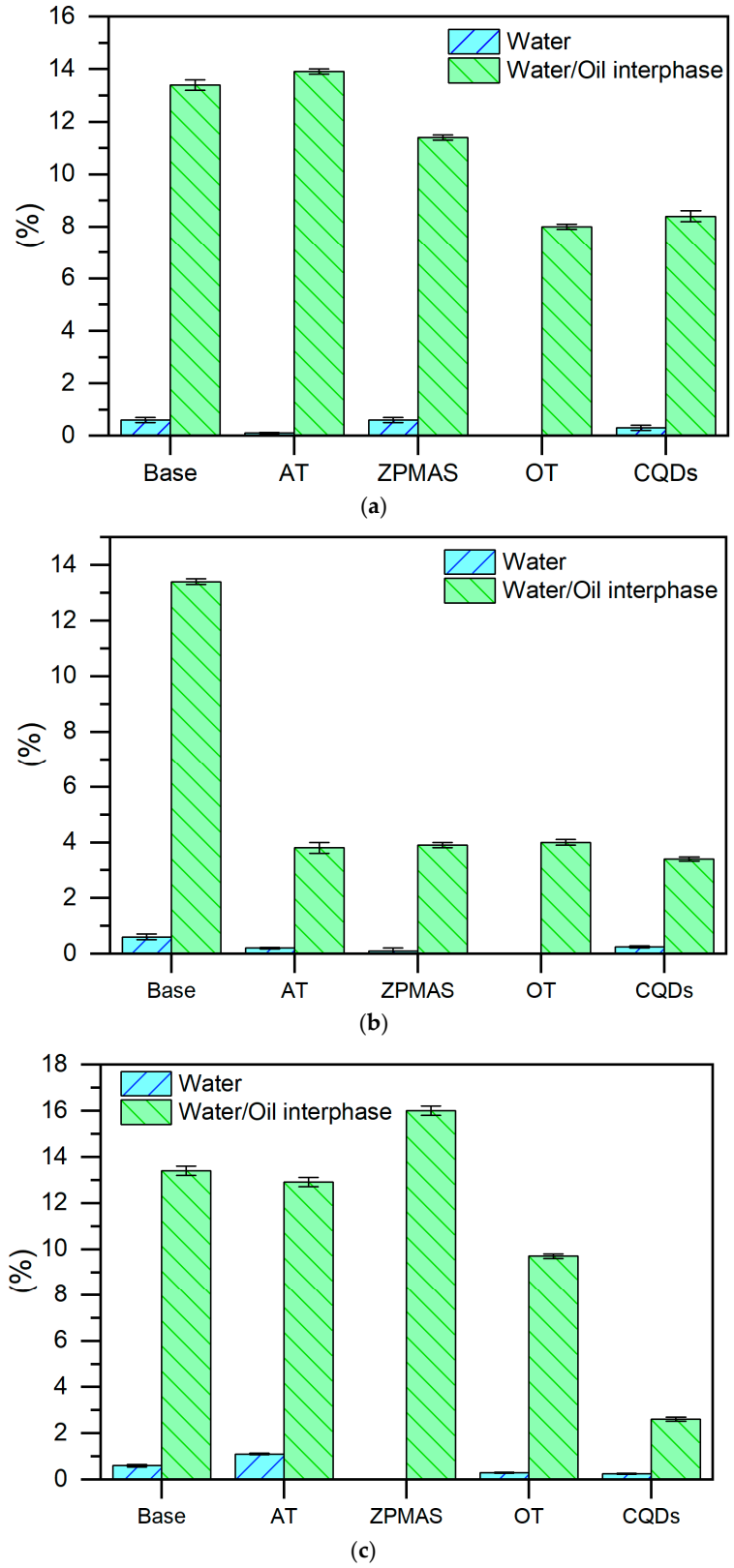
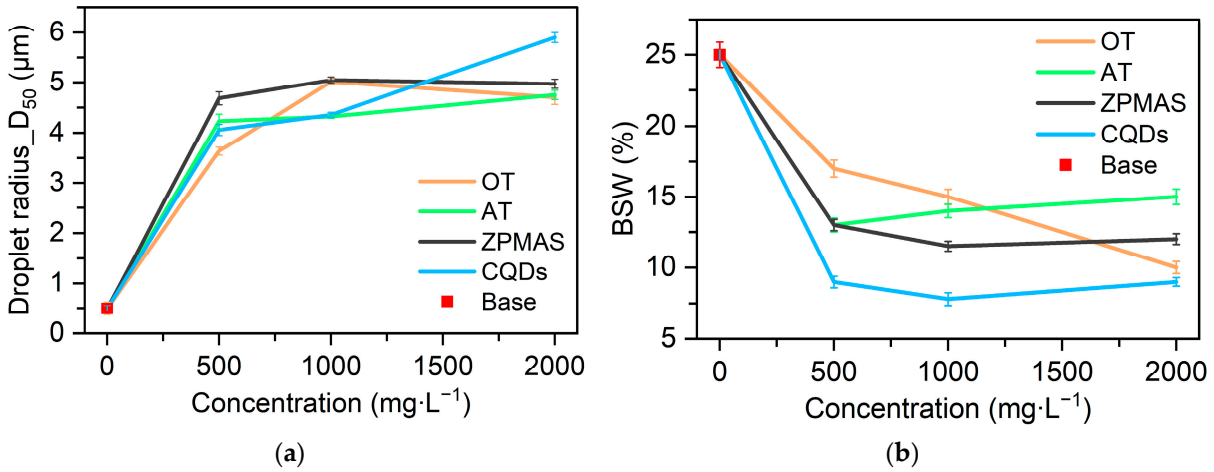


Figure 8. Percentage of water and water/crude oil interphase in the oil phase at different treatment concentrations (OT, ZPMAS, and AT) of (**a**) 500, (**b**) 1000, and (**c**) 2000 mg·L^{-1} under the mechanical separation scenario. Each system is compared with the base emulsion with no demulsifier treatment addition.

3.2.2. Thermal Separation Scenario

Figure 9 illustrates the droplet radius and BSW variations in the emulsion under the thermal separation scenario for the base emulsion and the systems including the conventional treatments (ZPMAS, AT, and OT) or the new treatment called blue CQDs. As described in the previous section, the treatments were evaluated at 500, 1000, and 2000 mg·L^{-1}. However, at this stage, the protocols incorporated temperature-based separation while avoiding centrifugal separation. The base emulsion, without adding a demulsifier, presented an average droplet radius (D_{50}), a BSW%, and remotion efficiencies of 0.5 µm, 25%, and 50%, respectively.



(**a**) (**b**)

Figure 9. (**a**) Average droplet radius (D_{50}) and (**b**) BSW% of the oil phase as a function of the treatment concentration for the conventional treatments OT, ZPMAS, AT, and blue CQDs under the thermal separation scenario. Base emulsion with no demulsifier treatment addition is also shown at a concentration of 0 mg·L^{-1}.

All three conventional treatments, OT, AT, and ZPMAS, showed a consistent increase in the radius of water droplets in the oil phase when the treatment concentration was increased from 500 to 1000 mg·L^{-1}. This indicates that, within this concentration range, the treatments contributed to larger droplets in the emulsion. Interestingly, the droplet radius decreased at 2000 mg·L^{-1} for OT and ZPMAS, suggesting that higher concentrations reduced droplet size. However, AT exhibits an anomaly when the droplet size is increased to 2000 mg·L^{-1}. In contrast to conventional treatments, the droplet size under the new treatment with blue CQDs continuously increased at higher concentrations. The droplet size was the largest at the highest concentration of 2000 mg·L^{-1}.

The initial increase in droplet size from 500 to 1000 mg·L^{-1} may be attributed to changes in the emulsifier behavior or interactions with the water and crude oil components. The subsequent decrease in droplet size at 2000 mg·L^{-1} (except for AT) suggests a concentration-dependent effect, in which the treatments may reach an optimal range for droplet stabilization.

With CQDs, the continuous increase in droplet size with increasing concentration indicates a different behavior compared to conventional treatments, achieving the highest water droplet radius at 2000 mg·L^{-1} (5.9 µm). This might be due to the properties or interactions of the blue CQDs with emulsion components. CQDs have a unique chemical composition that might interact differently with the water and crude oil phases in the emulsion compared with the chemical composition of conventional treatments. The nanometric size, surface chemistry, functional groups, and molecular structure of CQDs can influence their interactions with emulsion components [71–79]. CQDs affect water droplet coalescence

owing to their surface hydrophilic nature and nanometric size, contributing to the increase in the water droplet size because CQDs might be adsorbed at the interface of water droplets serving as coalescence points of water droplets [110]. In addition, the continuous increase in droplet size with increasing concentration of CQDs suggests concentration-dependent behavior.

Note that under the thermal separation, ZPMAS treatment at low concentrations (500 and 1000 mg·L^{-1}) exhibited lower BSW% values and higher removal efficiency values of 74% and 77%, respectively, regarding the other conventional treatments (OT and AT) and better performance concerning the scenario with mechanical separation, which could be explained due to a probably slower action of ZPMAS treatment regarding the other conventional treatments, and a demulsification mechanism based on the emulsion destabilization through the destabilization of inorganic solids by reducing the zeta potential and favoring flocculation [115], and the promotion of coalescence of water droplets through the effect of surfactant compounds, which favors the separation process [116]. Considering the BSW% of the oil phase (panel b), the blue CQDs significantly and consistently reduced the BSW% across all concentrations. The BSW values were 9%, 8%, and 9% at 500, 1000, and 2000 mg·L^{-1}, respectively, which represent remotion efficiency values of 82%, 84%, and 82%, respectively. This suggests that blue CQDs are particularly effective in minimizing water and sediment content in the emulsions exhibiting higher removal efficiencies, which are much greater than the base emulsion (50%). In contrast to ZPMAS, AT, and OT, which maintained BSW% values higher than 12% at all concentrations, blue CQDs consistently outperformed in reducing BSW. The distinctive behavior of the blue CQDs in reducing BSW may be attributed to their specific chemical, physical, or surface properties. CQDs probably act through three main mechanisms. (i) The location of the W/O interface: The high surface hydrophilicity and activity of CQDs because of the abundance of -OH, NH_2, and -COOH functional groups promotes dewatering [117,118], making them suitable for reaching the W/O interface and increasing the interfacial film rupture by adsorbing in the interfacial film competing against asphaltenes and resins, which promotes the displacement of these natural interfacial film stabilizers from the interface film and stimulates the coalescence of dispersed water droplets [17,111]. This mechanism was experimentally observed in this study, since after 3 h in the oven at 67.2 °C, the CQDs acted in the emulsion by coalescing the water bubble droplets, which were later deposited at the bottom of the recipient. (ii) The destabilization of fine solids: The acidic character of CQDs may destabilize fine solids, facilitating their removal from crude oil. This occurs because inorganic solids, such as silica in Pickering W/O emulsions, become unstable under acidic conditions (pH < 4.2) [11], leading to a reduction in electrostatic repulsion forces between solids. Additionally, CQDs may promote the destabilization of inorganic fine solids by altering their wettability. It is well known that CQDs can modify the surface properties of solids, shifting them from oil-wet to water-wet conditions [81,82]. Therefore, altering the wettability of the stabilizing particles might lead to a lower affinity of fine solids for the interfacial film withdrawing from the interface and, therefore, a reduction in their potential interaction at the interfacial film, which reduces the interfacial film strength [83] because fine hydrophobic solids that might stabilize the W/O emulsion by strengthening the interfacial film [24,26,27,103] are originally hydrophilic. (iii) Increasing the heat transfer efficiency: CQDs can enhance the thermal conductivity (k) and convective heat transfer coefficient (h) of fluids when incorporated into different systems [84]. This improvement can significantly accelerate the demulsification kinetics during heat treatment by increasing heat transfer efficiency. As a result, interfacial rigidity is reduced, and the frequency of water droplet collisions increases, promoting coalescence and accelerating water–oil phase separation [17,119]. Additionally, due to their nanometric size and high surface area, CQDs may further intensify these

effects, enhancing overall process efficiency [67,120]. Figure 10 briefly summarizes the above three mechanisms through a schematic representation. The use of blue CQDs as an emulsion treatment appears promising, especially considering their superior effectiveness in reducing BSW compared with the conventional treatments evaluated in this study.

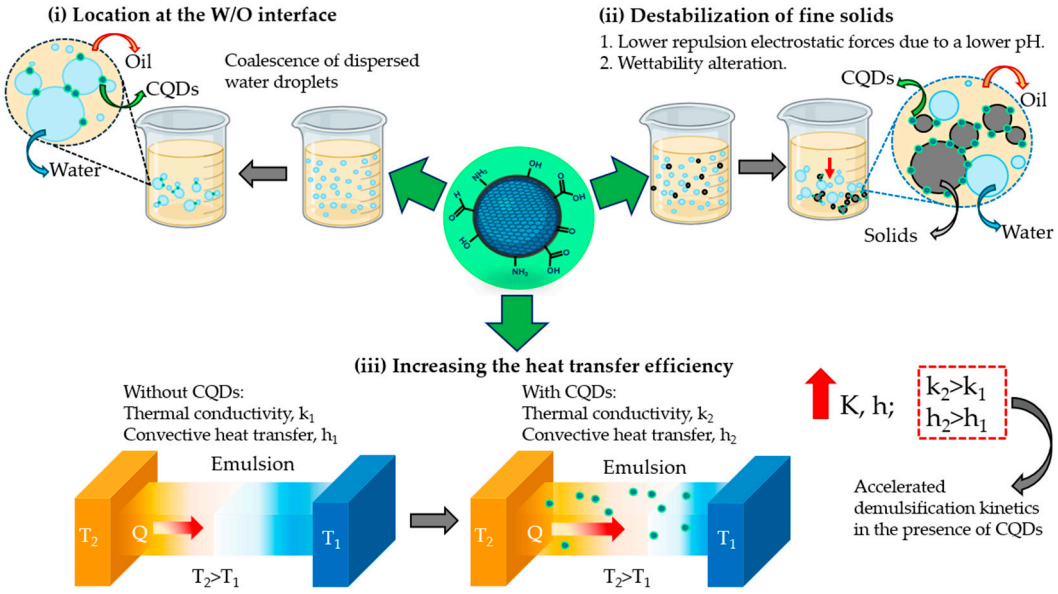


Figure 10. Schematic representation of the three main demulsification mechanisms of the CQDs: (**i**) location of the W/O interface and coalescence of water droplets, (**ii**) destabilization of fine solids, and (**iii**) increasing the heat transfer efficiency.

Figure 11 depicts the distribution of the three phases in the oil phase after basic sediment and water (BSW) measurements. These phases were solids, water, and a water/crude oil interphase. Compared to the untreated crude oil scenario, all demulsifier treatments generally reduce the water/crude oil interphase. This reduction indicates effective emulsion breaking, highlighting the efficacy of the applied demulsifiers. The influence of the treatments on solids and water content is also noteworthy. Note that solids were reduced when the concentration of the treatments was increased in all cases. This can be explained in terms of the emulsion pH resulting after the treatments are added at each concentration because, according to Derjaguin, Landau, Vervey, and Overbeek (DLVO) theory, the remaining inorganic solids of silica are unstable at acidic pH values lower than 4.2. At a specific pH value of 2.2, these solids reach the point of maximum instability in the emulsion because it is the isoelectric point of silica [11]. Furthermore, a lower pH resulting from a higher treatment concentration might also lead to higher dissolution of calcite solids [121]. While most treatments decreased the quantity of solids and water, an exception was observed in the case of 1000 and 2000 $mg \cdot L^{-1}$ ZPMAS, which increased the water content but reduced the water/oil interphase. This distinction emphasizes the nuanced effects of different demulsifiers at various concentrations [112].

A significant finding was the superior performance of the homemade treatment composed of blue CQDs. At all tested concentrations, CQDs consistently demonstrated superior performance in reducing solids, water content, and the water/crude oil interphase, indicating their exceptional effectiveness in breaking the emulsion. Furthermore, a concentration-dependent analysis revealed that 1000 $mg \cdot L^{-1}$ was the optimal concentration for CQDs among the tested concentrations. At this concentration, the emulsion-breaking efficiency is optimized, ensuring minimal levels of solids (<1%), water (<2%), and the water/crude oil interphase (<6%).

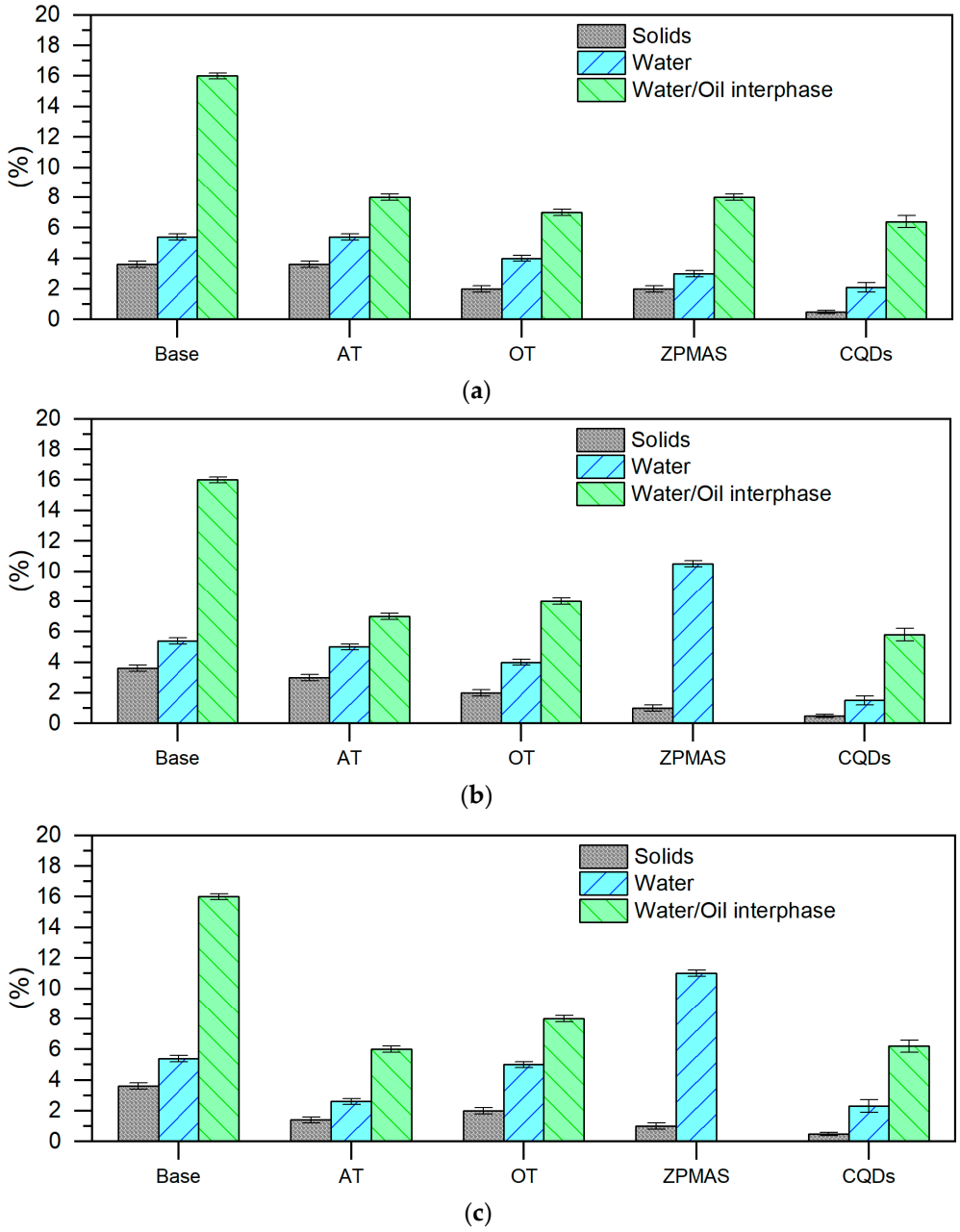


Figure 11. Percentage of water, solids, and water/crude oil interphase in the oil phase at treatment concentrations (OT, ZPMAS, AT, and CQDs blue) of (**a**) 500, (**b**) 1000, and (**c**) 2000 mg·L^{-1} under the thermal separation scenario. Each system is compared with the base emulsion, which has no demulsifier treatment addition.

The influence of the temperature and mechanical methods on the emulsion-breaking process is noteworthy. Comparatively, the effect of temperature on emulsion breakage appears less significant. While temperature contributes to the demulsification process, mechanical separation has a more pronounced impact on achieving greater phase separation.

When using the mechanical separation, the basic sediment and water (BSW%) percentage significantly decreases, along with the amounts of solids, water, and the water/crude oil interphase. This suggests that the mechanical method is highly effective in disrupting the emulsion and separating the different phases in the crude oil. The reduction in BSW% is a crucial indicator of improved separation efficiency.

Interestingly, the mechanical method not only reduced the BSW%, but also significantly increased the droplet size. This suggests that the mechanical forces applied during the

process lead to the coalescence or agglomeration of droplets, contributing to more efficient phase separation, as reported by Kokal et al. [122].

3.2.3. Thermomechanical Separation Scenario

Figure 12 provides insights into the droplet size over 6 h (panel a), basic sediment and water (BSW%) levels (panel b), and the distribution of water/oil interphase, water, and solids in the oil phase (panel c) based on the thermomechanical method for the base emulsion without adding chemical demulsifiers and systems at a fixed concentration of 1000 mg·L^{-1} for ZPMAS, AT, OT, and CQDs. The first graph shows the evolution of the droplet radius over time. Notably, the final droplet radius increased in the order Base (without treatments) < AT < ZPMAS < OT< CQDs. This suggests that CQD treatment is particularly effective in increasing the droplet size, indicating a superior emulsion-breaking capability, as discussed previously. The descending order aligns with the expected performance based on previous analyses, emphasizing the consistency of the CQDs in enhancing emulsion breaking. Conversely, the BSW% trend follows the opposite order, demonstrating a decrease in BSW% in the order of Base > AT > ZPMAS > OT> CQDs, with removal efficiency values increasing in the order 68% < 76% < 89% < 90% < 96%, respectively. The inverse relationship between droplet size and BSW% aligns with expectations, as smaller droplets contribute to increased emulsion stability and a higher BSW% [11,12]. The lower BSW% of the CQDs further supports their efficacy in emulsion breakage, reinforcing their potential for practical applications. The third graph reveals a considerable decrease in the concentrations of all phases when applying the combined mechanical and thermal methods compared with the base system. The reduction in phases follows the order AT < ZPMAS < OT < CQDs, with the system treated with CQDs demonstrating the most significant decrease. BSW values below 2% in the CQD-treated system indicate a highly effective emulsion-breaking capability, consistent with the trends observed in droplet size and BSW%. Note that although the CQDs performed better in reducing the phases, the OT system presented slightly lower fractions of solids than the CQDs, which indicates a better performance of OT in reducing solids. Furthermore, ZPMAS and CQDs are the most effective treatments for reducing the water phase as observed in Figure 12c with the lowest percentages of water.

Combining mechanical and thermal methods in the demulsification process likely produces better results than individual methods, owing to synergistic effects and complementary mechanisms. Both techniques add energy to the system, facilitating emulsion breakdown and promoting the separation of the water and oil phases.

A comprehensive analysis of the demulsification process in crude oil strongly suggests the implementation of a combined method involving both mechanical and thermal approaches [122]. This combination has consistently shown superior results in increasing droplet size, decreasing basic sediment and water (BSW%) levels, and decreasing the concentrations of phases in the crude oil compared to the individual methods; even when in the combined method (thermomechanical), the time of centrifugation and temperature decreased with respect to the individual methods. This behavior can be further supported by comparing the removal efficiencies because the removal efficiency ranges for the three scenarios increased in the order thermal (50–84%) < mechanical (68–92%) < and thermomechanical (68–96%).

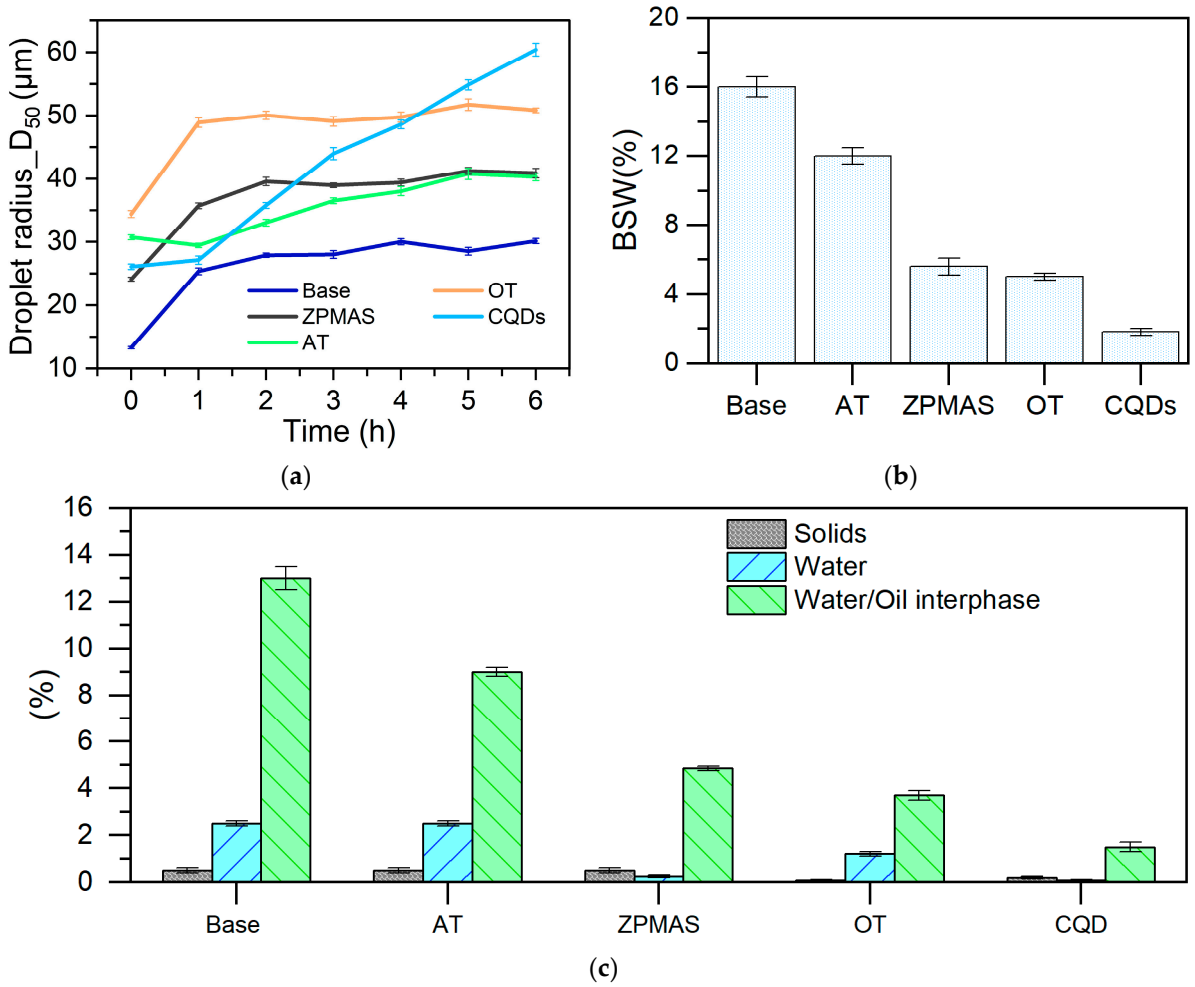


Figure 12. (**a**) Average droplet radius (D_{50}), (**b**) BSW%, and (**c**) percentage of solids, water, and water/crude oil interphase in the oil phase for the systems with treatments (AT, ZPMAS, OT, and blue CQDs) at 1000 mg·L^{-1} under the thermomechanical separation scenario. Each system is compared with the base emulsion, which has no demulsifier treatment addition.

Furthermore, the findings indicate that a concentration of 1000 mg·L^{-1} for demulsifying treatments, specifically ZPMAS, AT, OT, and CQDs, is optimal to achieve the most effective emulsion breaking. This concentration has consistently demonstrated superior results across various metrics, including droplet size reduction, lower BSW%, and decreased phase concentrations.

An additional avenue for exploration is to evaluate the synergistic effects of combining different treatments. Since individual treatments have shown unique strengths in demulsification, combining them could further enhance their effectiveness. This synergistic approach has the potential to yield results that surpass the efficacy of any single treatment, providing a promising direction for future research and practical applications in the oil industry.

3.3. Optimization of Demulsifier Treatment Based on a Simplex-Centroid Mixture Design

The optimum demulsifier was designed considering BSW% as the response variable. A total of seven systems were evaluated. The first three are covered in the previous section, and the remaining three are covered in this section. The binary and ternary treatments consisted of 500 mg·L^{-1} CQDs + 500 mg·L^{-1} ZPMAS, 500 mg·L^{-1} CQDs + 500 mg·L^{-1} OT, 500 mg·L^{-1} OT + 500 mg·L^{-1} ZPMAS, and mg·L^{-1}CQDs + 333 mg·L^{-1} ZPMAS + 333 mg·L^{-1} OT. The systems were integrated based on the SCMD, as shown in Figure 3.

The droplet size and distribution of solids, water, and water/crude oil interphase in the oil phase were also analyzed, as presented in Figure 13, for the overall behavior of the designed treatments. The droplet size increased over 6 h of heating, aligning with the trend observed in individual treatments. However, the final droplet size of the water droplets was notably larger for the combined demulsifier treatments. The order of final droplet sizes after 6 h at 67.2 °C was 500 mg·L^{-1} OT + 500 mg·L^{-1} ZPMAS < 500 mg·L^{-1} CQDs + 500 mg·L^{-1} ZPMAS < 333 mg·L^{-1} CQDs + 333 mg·L^{-1} ZPMAS + 333 mg·L^{-1} OT < 500 mg·L^{-1} CQDs + 500 mg·L^{-1} OT, with sizes of 52, 58, 60, and 63 µm, respectively. The reduction in BSW% followed a similar order, with the highest remotion efficiency values (98% and 99%) observed in the systems containing 333 mg·L^{-1} CQDs + 333 mg·L^{-1} ZPMAS + 333 mg·L^{-1} OT and 500 mg·L^{-1} CQDs + 500 mg·L^{-1} OT, achieving BSW% values of 1.0% and 0.5%, respectively. Note that the BSW obtained for the system, including 500 mg·L^{-1} CQDs + 500 mg·L^{-1} OT, is the maximum value accepted for crude oils for sale and transport and is considered a perfect separation value for dehydrated crude oil [123]. Finally, the order of BSW% reduction aligns with the order of the droplet radius, suggesting a correlation between the droplet size and BSW%.

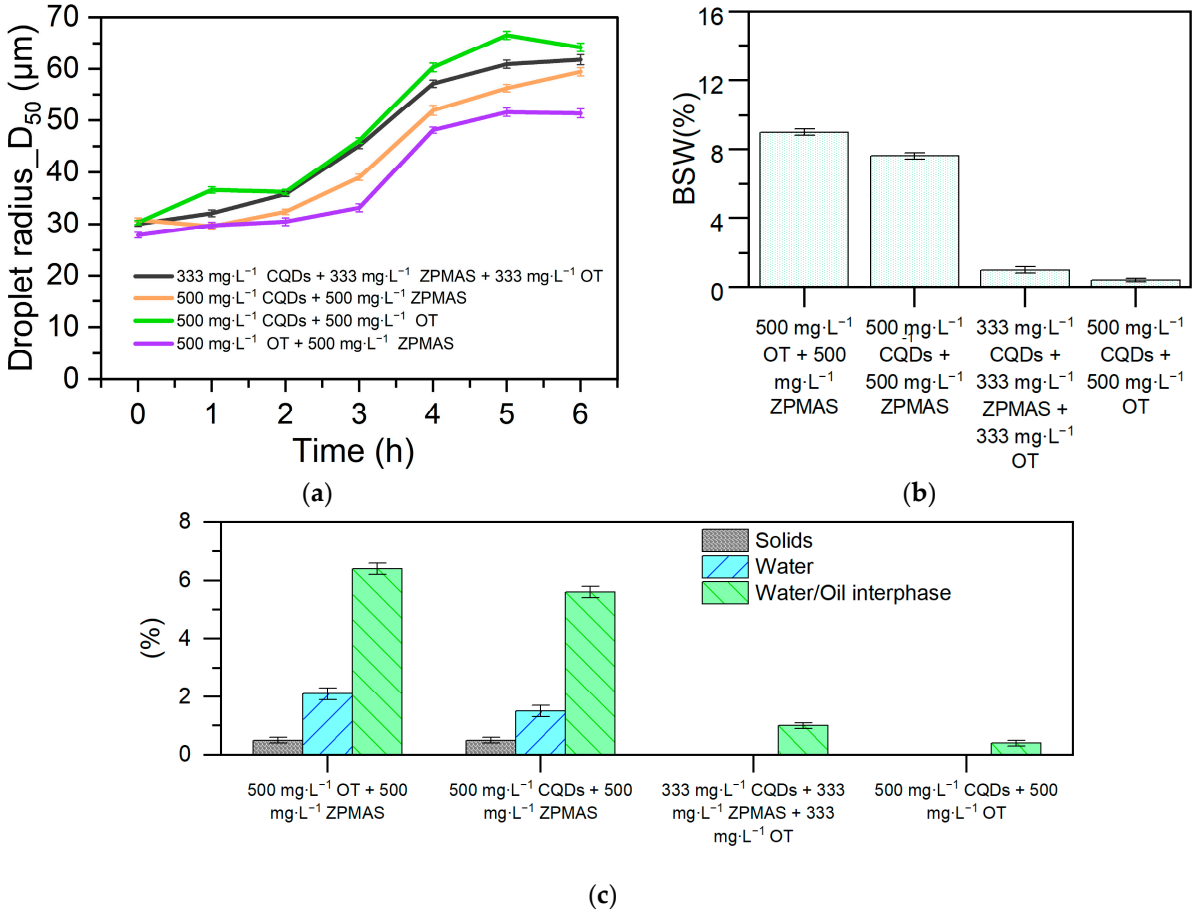


Figure 13. (**a**) Average droplet radius (D_{50}), (**b**) BSW%, and (**c**) percentage of solids, water, and water/crude oil interphase in the oil phase for the systems with a mixture of treatments (ZPMAS, OT, and CQDs blue) at a total concentration of 1000 mg·L^{-1} under the thermomechanical separation scenario.

Both solid and water contents were reduced to 0% in the presence of 333 mg L^{-1} CQDs + 333 mg·L^{-1} ZPMAS + 333 mg·L^{-1} OT and 500 mg·L^{-1} CQDs + 500 mg·L^{-1} OT. This indicates that these demulsifier combinations effectively eliminated solids and water content from the crude oil phase. Also, the water/crude oil interphase was below 1% in samples mixed with both systems. The synergistic effect between treatments can be

explained as CQDs significantly reducing the water/oil interphase and water phases. At the same time, ZPMAS also contributed to emulsion destabilization and decreased the water phase. In comparison, OT performed better at reducing solids.

STATGRAPHICS Centurion XVI software was used to obtain statistical results following the experimental mixture design described in Section 2.3 and using the previous experimental data of BSW% condensed in Figures 12 and 13. The results were validated using a special cubic model with an $R^2 > 0.99$. The maximum reduction in the BSW% was predicted by considering the composition of the demulsifiers ZPMAS, OT, and CQDs. Table 4 lists the β values of the BSW% model as a function of the pseudo-components, ZPMAS, OT, and CQDs. The optimal point for BSW reduction was found for treatment containing 500 mg·L^{-1} CQDs, 380 mg·L^{-1} OT, and 120 mg·L^{-1} ZPMAS. Figure 14 shows the response surface of the BSW% resulting in the crude oil phase after treatment with demulsifiers containing ZPMAS-OT-CQDs. It is worth mentioning that the optimum treatment was experimentally evaluated, obtaining 0% BSW, droplet sizes higher than 70 μm, and the elimination of the solids, water, and water/crude oil interphase.

Table 4. Calculated parameters of the special cubic model for the BSW% of an emulsion with different mixtures of treatments (ZPMAS, OT, and blue CQDs) under the thermomechanical scenario.

β_1	β_2	β_3	β_{12}	β_{13}	β_{23}	β_{123}	R^2
5.6	1.8	5.0	15.6	14.8	−12	−139.8	0.99

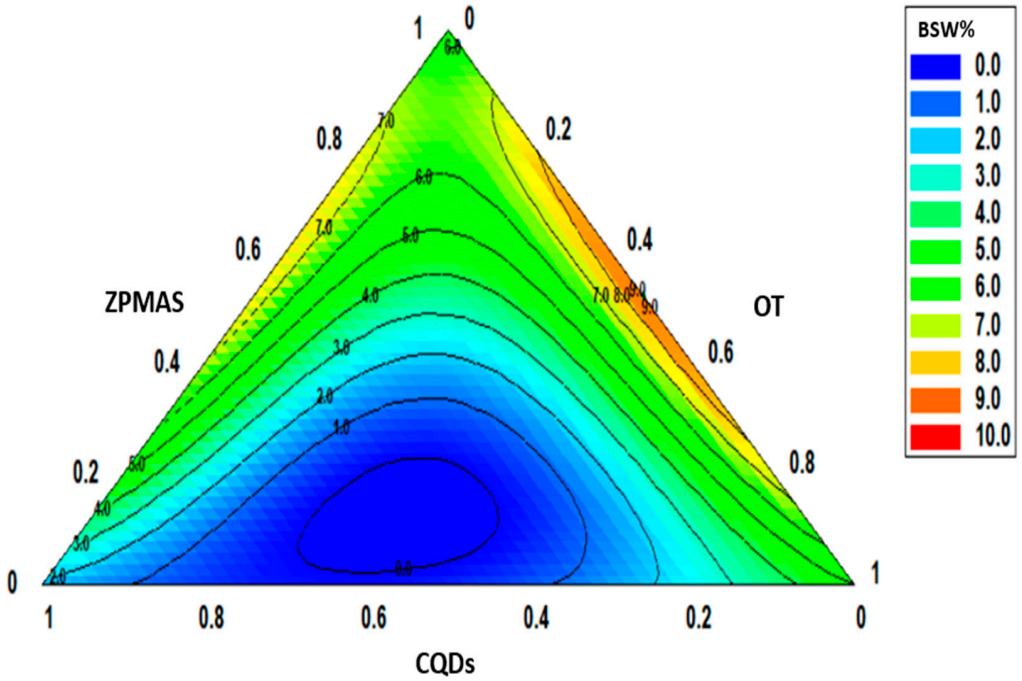


Figure 14. Response surface for the BSW% response variable in systems with a mixture of treatments (ZPMAS, OT, and blue CQDs) under the thermomechanical separation scenario.

Note that the optimal point obtained from the response surface comprised three chemical treatments (500 mg·L^{-1} CQDs + 380 mg·L^{-1} OT + 120 mg·L^{-1} ZPMAS), a formulation with an HLB number of 9.1, which is higher than the minimum HLB number for W/O demulsifiers, which is 8.0 [17,19]. This supports the performance of the novel CQD-enhanced demulsifier. Therefore, in the final formulation, ZPMAS mainly acts as a solid flocculant, favoring the instability and posterior removal of fine solids from the W/O interface, which reduces the interfacial film strength [47] and facilitates the higher

adsorption of surfactant molecules from OT and CQDs at the W/O interface, leading to the coalescence and flocculation of dispersed water droplets [17,111]. Furthermore, OT acts as a carrier and solvent for natural interfacial film stabilizers, such as resins and asphaltenes, displacing them from the W/O interface [49,109]. However, as previously mentioned, CQDs probably act through three main mechanisms. (i) The location of the W/O interface and increasing of the interfacial film rupture by adsorbing in the interfacial film and promoting the displacement of these natural interfacial film stabilizers from the interface film stimulates the coalescence of dispersed water droplets [17,111]. (ii) The destabilization of fine solids: The acidic character of CQDs might promote the removal of solids from crude oil because inorganic solids such as silica are unstable at a pH lower than 4.2 [11]. CQDs can also alter the wettability of solids from oil-wettable to water-wettable [81,82], thereby reducing their affinity for the W/O interface and decreasing the interfacial film strength [83]. (iii) Increasing the thermal conductivity of the emulsion: Adding CQDs can promote an increase in the thermal conductivity of the emulsion [84], which can notably enhance the demulsification process when heat treatment is applied by favoring less rigidity of the interfacial film and higher collisions between the water droplets, leading to the coalescence of the dispersed water droplets [17,119].

It is also worth noting that using the CQD-enhanced demulsifier at the optimal point of the SCMD reduces the quantity of other active ingredients (OT and ZPMAS), which is favorable because CQDs are usually eco-friendlier and more cost-efficient than conventional chemical treatments with complex chemistry that enhances production costs [67,124]. Moreover, implementing CQDs might be a more promising and cost-efficient route to address the actual need for complex nanomaterials by functionalizing nanomaterials and/or fabricating core–shell or GO nanomaterials [4,57–65]. Finally, it should be noted that to obtain a BSW < 0.1%, the use of the CQD-enhanced demulsifier at the optimal point of the SCMD in conjunction with the thermomechanical treatment significantly reduced the centrifugation time (15 min) by 95.8% in the initial scenario without adding chemicals and without applying heat in the characterization stage (6 h). In addition, it should also be noted that the use of the CQD-enhanced demulsifier at the optimum point of the SCMD under the thermomechanical treatment reduces the centrifugation and the heating times in the mechanical and the thermal scenarios, obtaining lower BSW values and time reductions of 25.0% and 37.5%, respectively. This is a crucial result because these time reductions represent lower operation times for centrifuges and ovens. This is positive because high operation times are a limiting factor at the industrial scale [124].

4. Conclusions

This study optimizes crude oil demulsification through a combined mechanical and thermal approach, emphasizing the synergistic effects of demulsifiers. Various treatments were evaluated at different concentrations, including conventional demulsifiers (ZPMAS, AT, and OT) and novel blue carbon quantum dots (CQDs). Regardless of the treatment, an optimal concentration of 1000 $mg \cdot L^{-1}$ consistently improved emulsion breaking. Synergistic demulsifier combinations, designed using SCMD methodology, significantly enhanced performance by increasing water droplet size, reducing BSW%, and eliminating unwanted crude oil-like solids. The optimal formulation—500 $mg \cdot L^{-1}$ CQDs + 380 $mg \cdot L^{-1}$ OT + 120 $mg \cdot L^{-1}$ ZPMAS—achieved the highest demulsification efficiency. Incorporating CQDs reduced reliance on conventional demulsifiers with complex chemistry and higher costs, leading to more sustainable and cost-effective solutions while improving overall separation efficiency.

These findings have important implications for the oil industry, highlighting the potential of CQDs to enhance demulsifier performance while reducing environmental

impact. Future research should explore the influence of different CQD properties, such as fluorescent emission (blue, green, yellow, red) and nanometric size, as well as the effects of varying temperature conditions and industrial-scale applications.

Supplementary Materials: The following supporting information can be downloaded at https://www.mdpi.com/article/10.3390/pr13020575/s1: Figure S1: Photographic record of the phases obtained from the emulsion after the BSW test (stirring at 4500 rpm for 10 min with 50% *v*/*v* toluene). Phase 1: Crude oil; Phase 2: crude oil/ water interphase; Phase 3: deposit solids; and Phase 4: water. Figure S2: Photographic record of (a) Phase 2 (crude oil/water interphase) and (b) Phase 3 (deposit solids) before and (c) after washing with organic solvents (toluene, heptane, and carbon disulfide). Figure S3: Fourier transform infrared (FTIR) spectrums for (a) conventional chemical demulsifiers (AT, OT, ZPMAS) and (b) CQDs.

Author Contributions: J.F.G.: conceptualization; data curation; formal analysis; investigation; methodology; software; validation; visualization; and writing—original draft. O.E.M.: conceptualization; data curation; formal analysis; investigation; software; validation; visualization; and writing—original draft. J.A.T.: conceptualization; methodology; and writing—reviewing and editing. C.M.: conceptualization; methodology; and writing—reviewing and editing. A.F.M.: writing—reviewing and editing. C.C.: writing—reviewing and editing. F.B.C.: conceptualization; formal analysis; and writing—reviewing and editing. C.A.F.: conceptualization; formal analysis; and writing—reviewing and editing. All authors have read and agreed to the published version of the manuscript.

Funding: This research received no external funding.

Data Availability Statement: The original contributions presented in this study are included in the article. Further inquiries can be directed to the corresponding author.

Acknowledgments: The authors acknowledge the Universidad Nacional de Colombia and Hocol. S.A. Financial and Technical Support.

Conflicts of Interest: Authors Jose A. Tengono, Camilo Mazo, Andres F. Maya, Cristina Caro were employed by Jefatura de Gestión de Activos, HOCOL S.A. The remaining authors declare that the research was conducted in the absence of any commercial or financial relationships that could be construed as a potential conflict of interest.

References

1. Faizullayev, S.; Adilbekova, A.; Kujawski, W.; Mirzaeian, M. Recent demulsification methods of crude oil emulsions—Brief review. *J. Pet. Sci. Eng.* **2022**, *215*, 110643. [CrossRef]
2. Medina, O.E.; Galeano-Caro, D.; Brattekås, B.; Pérez-Cadenas, A.F.; Carrasco-Marín, F.; Cortés, F.B.; Franco, C.A. Simultaneous CO_2 adsorption and conversion over Ni-Pd supported CeO_2 nanoparticles during catalytic n-C7 asphaltene gasification. *Fuel* **2023**, *342*, 127733. [CrossRef]
3. Medina, O.E.; Moncayo-Riascos, I.; Franco, C.A.; Cortés, F.B. Molecular Dynamic Simulation and Experiments on n-C7 Asphaltene Pyrolysis under High-Pressure Conditions Using Ceria-Based Nanocatalysts. *ACS Appl. Nano Mater.* **2023**, *6*, 12805–12815. [CrossRef]
4. Fang-Hui, W.; Hong, Z. The Application and Research of Dispersing In Situ Nano-SiO_2 in Polyether Demulsifier TA1031. *J. Dispers. Sci. Technol.* **2008**, *29*, 1081–1084. [CrossRef]
5. Wang, D.; Yang, D.; Huang, C.; Huang, Y.; Yang, D.; Zhang, H.; Liu, Q.; Tang, T.; El-Din, M.G.; Kemppi, T. Stabilization mechanism and chemical demulsification of water-in-oil and oil-in-water emulsions in petroleum industry: A review. *Fuel* **2021**, *286*, 119390. [CrossRef]
6. Wu, J.; Xu, Y.; Dabros, T.; Hamza, H. Effect of demulsifier properties on destabilization of water-in-oil emulsion. *Energy Fuels* **2003**, *17*, 1554–1559. [CrossRef]
7. Medina, O.E.; Galeano-Caro, D.; Ocampo-Pérez, R.; Perez-Cadenas, A.F.; Carrasco-Marín, F.; Franco, C.A.; Corteś, F.B. Development of a monolithic carbon xerogel-metal composite for crude oil removal from oil in-saltwater emulsions: Evaluation of reuse cycles. *Microporous Mesoporous Mater.* **2021**, *327*, 111424. [CrossRef]

8. Medina, O.E.; Galeano-Caro, D.; Castelo-Quibén, J.; Ocampo-Pérez, R.; Perez-Cadenas, A.F.; Carrasco-Marín, F.; Franco, C.A.; Corteś, F.B. Monolithic carbon xerogels-metal composites for crude oil removal from oil in-saltwater emulsions and subsequent regeneration through oxidation process: Composites synthesis, adsorption studies, and oil decomposition experiments. *Microporous Mesoporous Mater.* **2021**, *319*, 111039. [CrossRef]
9. Acosta, L.; Galeano-Caro, D.; Medina, O.E.; Cortés, F.B.; Franco, C.A. Nano-intermediate of magnetite nanoparticles supported on activated carbon from spent coffee grounds for treatment of wastewater from oil industry and energy production. *Processes* **2020**, *9*, 63. [CrossRef]
10. López, D.; Zabala, R.D.; Matute, C.; Lopera, S.H.; Cortés, F.B.; Franco, C.A. Well injectivity loss during chemical gas stimulation process in gas-condensate tight reservoirs. *Fuel* **2021**, *283*, 118931. [CrossRef]
11. Dyab, A.K.F. Destabilisation of Pickering emulsions using pH. *Colloids Surf. A Physicochem. Eng. Asp.* **2012**, *402*, 2–12. [CrossRef]
12. Dapčević Hadnađev, T.; Dokić, P.; Krstonošić, V.; Hadnađev, M. Influence of oil phase concentration on droplet size distribution and stability of oil-in-water emulsions. *Eur. J. Lipid Sci. Technol.* **2013**, *115*, 313–321. [CrossRef]
13. Bourrel, M.; Passade-Boupat, N. Crude oil surface active species: Consequences for enhanced oil recovery and emulsion stability. *Energy Fuels* **2017**, *32*, 2642–2652. [CrossRef]
14. Dickinson, E. Use of nanoparticles and microparticles in the formation and stabilization of food emulsions. *Trends Food Sci. Technol.* **2012**, *24*, 4–12. [CrossRef]
15. Rayner, M.; Marku, D.; Eriksson, M.; Sjöö, M.; Dejmek, P.; Wahlgren, M. Biomass-based particles for the formulation of Pickering type emulsions in food and topical applications. *Colloids Surf. A Physicochem. Eng. Asp.* **2014**, *458*, 48–62. [CrossRef]
16. Xiao, J.; Li, C.; Huang, Q. Kafirin Nanoparticle-Stabilized Pickering Emulsions as Oral Delivery Vehicles: Physicochemical Stability and in Vitro Digestion Profile. *J. Agric. Food Chem.* **2015**, *63*, 10263–10270. [CrossRef]
17. Alara, O.R.; Abdurahman, N.H.; Tade, M.O.; Ali, H.A.; Alao, K.T. Demulsifier: An Important Agent in Breaking Crude Oil Emulsions. *Chem. Eng. Technol.* **2022**, *45*, 1707–1720. [CrossRef]
18. Zolfaghari, R.; Fakhru'l-Razi, A.; Abdullah, L.C.; Elnashaie, S.S.E.H.; Pendashteh, A. Demulsification techniques of water-in-oil and oil-in-water emulsions in petroleum industry. *Sep. Purif. Technol.* **2016**, *170*, 377–407. [CrossRef]
19. Adeyanju, O.A.; Oyekunle, L.O. Optimum demulsifier formulations for Nigerian crude oil-water emulsions. *Egypt. J. Pet.* **2018**, *27*, 657–662. [CrossRef]
20. Sjoblom, J. *Encyclopedic Handbook of Emulsion Technology*; CRC Press: Boca Raton, FL, USA, 2001.
21. Udonne, J.D. Chemical treatment of emulsion problem in crude oil production. *J. Pet. Gas Eng.* **2012**, *7*, 135–141.
22. Auflem, I.H. Influence of Asphaltene Aggregation and Pressure on Crude Oil Emulsion Stability. Ph.D. Thesis, Norwegian University of Science and Technology, Trondheim, Norway, 2002.
23. Tiban Anrango, B.A.; Naiya, M.M.; Van Dongen, J.; Matich, O.; Whitby, C.P.; Chen, J.L.Y. Nanoprecipitation to produce hydrophobic cellulose nanospheres for water-in-oil Pickering emulsions. *Cellulose* **2024**, *31*, 6225–6239. [CrossRef]
24. Umar, A.A.; Saaid, I.B.M.; Sulaimon, A.A.; Pilus, R.B.M. A review of petroleum emulsions and recent progress on water-in-crude oil emulsions stabilized by natural surfactants and solids. *J. Pet. Sci. Eng.* **2018**, *165*, 673–690. [CrossRef]
25. Yang, Y.; Fang, Z.; Chen, X.; Zhang, W.; Xie, Y.; Chen, Y.; Liu, Z.; Yuan, W. An Overview of Pickering Emulsions: Solid-Particle Materials, Classification, Morphology, and Applications. *Front. Pharmacol.* **2017**, *8*, 287. [CrossRef] [PubMed]
26. Binks, B.P.; Lumsdon, S.O. Catastrophic Phase Inversion of Water-in-Oil Emulsions Stabilized by Hydrophobic Silica. *Langmuir* **2000**, *16*, 2539–2547. [CrossRef]
27. Abdulredha, M.M.; Siti Aslina, H.; Luqman, C.A. Overview on petroleum emulsions, formation, influence and demulsification treatment techniques. *Arab. J. Chem.* **2020**, *13*, 3403–3428. [CrossRef]
28. Abed, S.M.; Abdurahman, N.H.; Yunus, R.M.; Abdulbari, H.A.; Akbari, S. Oil emulsions and the different recent demulsification techniques in the petroleum industry—A review. *IOP Conf. Ser. Mater. Sci. Eng.* **2019**, *702*, 012060. [CrossRef]
29. Kocherginsky, N.M.; Tan, C.L.; Lu, W.F. Demulsification of water-in-oil emulsions via filtration through a hydrophilic polymer membrane. *J. Membr. Sci.* **2003**, *220*, 117–128. [CrossRef]
30. Igunnu, E.T.; Chen, G.Z. Produced water treatment technologies. *Int. J. Low-Carbon Technol.* **2014**, *9*, 157–177. [CrossRef]
31. Bi, X.; Gu, Y.; Wang, K.; Jiang, M.; Xiao, P.; Luo, J.; Fang, W.; Liu, B. Demulsification of W/O emulsions induced by terahertz pulse electric fields-driven hydrogen bond disruption of water molecules. *Sep. Purif. Technol.* **2024**, *349*, 127819. [CrossRef]
32. Wang, B.-B.; Wang, X.-D.; Wang, T.-H.; Lu, G.; Yan, W.-M. Electro-coalescence of two charged droplets under constant and pulsed DC electric fields. *Int. J. Heat Mass Transf.* **2016**, *98*, 10–16. [CrossRef]
33. Kim, J.; Ahn, D.; Park, S.; Kim, W.J.; Ji, I.S.; Kang, J.-W.; Hong, J. Table-top numbering-up 3D-printed miniaturized hydrocyclone for high-efficiency and high-throughput separation of oil-in-water emulsions. *Sep. Purif. Technol.* **2024**, *336*, 126165. [CrossRef]
34. Li, W.; Ma, Y.; Feng, X.; Alheshibri, M.; Bu, X.; Ma, G.; Ni, M.; Li, Q.; Liu, A.; Niu, X. Optimization of an oil recovery process from oily sludge using a combined technique of froth flotation and centrifugal treatment. *J. Clean. Prod.* **2023**, *400*, 136752. [CrossRef]
35. Yao, L.; Selmi, A.; Esmaeili, H. A review study on new aspects of biodemulsifiers: Production, features and their application in wastewater treatment. *Chemosphere* **2021**, *284*, 131364. [CrossRef] [PubMed]

36. Li, Z.; Fuentes, J.; Chakraborty, A.; Zamora, E.; Prasad, V.; Vázquez, F.; Xu, Z.; Liu, Q.; Flores, C.; McCaffrey, W.C. Dehydration of water-in-crude oil emulsions using polymeric demulsifiers: A model for water removal based on the viscoelastic properties of the oil–water interfacial film. *Fuel* **2023**, *332*, 126185. [CrossRef]
37. Zhang, X.; He, C.; Zhou, J.; Tian, Y.; He, L.; Sui, H.; Li, X. Demulsification of water-in-heavy oil emulsions by oxygen-enriched non-ionic demulsifier: Synthesis, characterization and mechanisms. *Fuel* **2023**, *338*, 127274. [CrossRef]
38. You, Z.; Xu, H.; Sun, Y.; Zhang, S.; Zhang, L. Effective treatment of emulsified oil wastewater by the coagulation–flotation process. *RSC Adv.* **2018**, *8*, 40639–40646. [CrossRef] [PubMed]
39. Skale, T.; Hohl, L.; Kraume, M.; Drews, A. Feasibility of w/o Pickering emulsion ultrafiltration. *J. Membr. Sci.* **2017**, *535*, 1–9. [CrossRef]
40. Zhang, X.; Liu, C.; Yang, J.; Huang, X.-J.; Xu, Z.-K. Wettability Switchable Membranes for Separating Both Oil-in-water and water-in-oil emulsions. *J. Membr. Sci.* **2021**, *624*, 118976. [CrossRef]
41. Shih, S.S. Catalytic process for crude oil desalting. *J. Clean. Prod.* **1997**, *3*, 234.
42. Xu, X.; Yang, J.; Gao, J. Effects of demulsifier structure on desalting efficiency of crude oils. *Pet. Sci. Technol.* **2006**, *24*, 673–688. [CrossRef]
43. Romanova, Y.N.; Maryutina, T.A.; Musina, N.S.; Spivakov, B.Y. Application of ultrasonic treatment for demulsification of stable water-in-oil emulsions. *J. Pet. Sci. Eng.* **2022**, *209*, 109977. [CrossRef]
44. Díaz Velázquez, H.; Guzmán-Lucero, D.; Martínez-Palou, R. Microwave-assisted demulsification for oilfield applications: A critical review. *J. Dispers. Sci. Technol.* **2023**, *44*, 1884–1899. [CrossRef]
45. Ben Rejeb, Z.; Abidli, A.; Zaoui, A.; Fashandi, M.; Selka, A.; Naguib, H.E.; Park, C.B. One-pot synthesis of rationally-designed flexible, robust, and hydrophobic ambient-dried molecularly-bridged silica aerogels with efficient and versatile oil/water separation applications. *Adv. Compos. Hybrid Mater.* **2024**, *7*, 188. [CrossRef]
46. Yu, L.; Jia, Q.; Lu, C.; Chen, R. Photothermally responsive, magnetic and flame-retardant MOF-based polyurethane sponges for oil/water separation and emulsion purification. *Sep. Purif. Technol.* **2025**, *354*, 129088. [CrossRef]
47. Zhao, C.; Zhou, J.; Yan, Y.; Yang, L.; Xing, G.; Li, H.; Wu, P.; Wang, M.; Zheng, H. Application of coagulation/flocculation in oily wastewater treatment: A review. *Sci. Total Environ.* **2021**, *765*, 142795. [CrossRef]
48. Jiguang, L.; Xin, G.; Haiping, S.; Xinheng, C.; Ming, D.; Huandi, H. The solubility of asphaltene in organic solvents and its relation to the molecular structure. *J. Mol. Liq.* **2021**, *327*, 114826. [CrossRef]
49. Juan, P.; Ingrid, V.; Ronald, B.; Meraldo, S.; César, P.; Carlos, C. Crude Oil Desalting Process. In *Advances in Petrochemicals*; Vivek, P., Ed.; IntechOpen: Rijeka, Croatia, 2015; Chapter 4.
50. Raya, S.A.; Mohd Saaid, I.; Abbas Ahmed, A.; Abubakar Umar, A. A critical review of development and demulsification mechanisms of crude oil emulsion in the petroleum industry. *J. Pet. Explor. Prod. Technol.* **2020**, *10*, 1711–1728. [CrossRef]
51. Schramm, L.L. Fundamentals and applications in the petroleum Industry. *Adv. Chem* **1992**, *231*, 3–24.
52. Cheng, Q.; Cao, G.; Bai, Y.; Zhu, Z.; Zhang, N.; Li, D. Probing the Demulsification Mechanism of Emulsion with SPAN Series Based on the Effect of Solid Phase Particles. *Molecules* **2023**, *28*, 3261. [CrossRef] [PubMed]
53. Liu, J.; Wang, H.; Li, X.; Jia, W.; Zhao, Y.; Ren, S. Recyclable magnetic graphene oxide for rapid and efficient demulsification of crude oil-in-water emulsion. *Fuel* **2017**, *189*, 79–87. [CrossRef]
54. Nikkhah, M.; Tohidian, T.; Rahimpour, M.R.; Jahanmiri, A. Efficient demulsification of water-in-oil emulsion by a novel nano-titania modified chemical demulsifier. *Chem. Eng. Res. Des.* **2015**, *94*, 164–172. [CrossRef]
55. Xie, H.; Zhao, W.; Zhang, X.; Wang, Z. Demulsification of Bacteria-Stabilized Pickering Emulsions Using Modified Silica Nanoparticles. *ACS Appl. Mater. Interfaces* **2022**, *14*, 24102–24112. [CrossRef] [PubMed]
56. Zhou, J.; Sui, H.; Ma, J.; Li, X.; Al-Shiaani, N.H.A.; He, L. Fast demulsification of oil-water emulsions at room temperature by functionalized magnetic nanoparticles. *Sep. Purif. Technol.* **2021**, *274*, 118967. [CrossRef]
57. Wang, F.; Shen, L.; Zhu, H.; Han, K. The preparation of a polyether demulsifier modified by Nano-SiO_2 and the effect on asphaltenes and resins. *Pet. Sci. Technol.* **2011**, *29*, 2521–2529. [CrossRef]
58. Peng, J.; Liu, Q.; Xu, Z.; Masliyah, J. Novel magnetic demulsifier for water removal from diluted bitumen emulsion. *Energy Fuels* **2012**, *26*, 2705–2710. [CrossRef]
59. Wang, B.; Wei, Y.; Wang, Q.; Di, J.; Miao, S.; Yu, J. Superhydrophobic magnetic core–shell mesoporous organosilica nanoparticles with dendritic architecture for oil–water separation. *Mater. Chem. Front.* **2020**, *4*, 2184–2191. [CrossRef]
60. Mao, X.; Wang, F.; Lu, B.; Tang, T.; Liu, Q.; Zeng, H. Novel polymer nanoparticles with core–shell structure for breaking asphaltenes-stabilized W/O and O/W emulsions. *J. Colloid Interface Sci.* **2023**, *640*, 296–308. [CrossRef]
61. Lü, T.; Wu, Y.; Qi, D.; Sun, Y.; Zhang, D.; Zhao, H. Fabrication of alkyl/amino siloxane-modified magnetic nanoparticles for simultaneous demulsification of O/W and W/O emulsions. *Colloids Surf. A Physicochem. Eng. Asp.* **2022**, *648*, 129295. [CrossRef]
62. Liu, J.; Li, X.; Jia, W.; Li, Z.; Zhao, Y.; Ren, S. Demulsification of crude oil-in-water emulsions driven by graphene oxide nanosheets. *Energy Fuels* **2015**, *29*, 4644–4653. [CrossRef]

63. Chen, Y.; Tian, G.; Liang, H.; Liang, Y. Synthesis of magnetically responsive hyperbranched polyamidoamine based on the graphene oxide: Application as demulsifier for oil-in-water emulsions. *Int. J. Energy Res.* **2019**, *43*, 4756–4765. [CrossRef]
64. Lowe, S.E.; Zhong, Y.L. Challenges of Industrial-Scale Graphene Oxide Production. In *Graphene Oxide*; John Wiley & Sons, Ltd.: Chichester, UK, 2017; Chapter 13; pp. 410–431. [CrossRef]
65. Farooq, U.; Patil, A.; Panjwani, B.; Simonsen, G. Review on Application of Nanotechnology for Asphaltene Adsorption, Crude Oil Demulsification, and Produced Water Treatment. *Energy Fuels* **2021**, *35*, 19191–19210. [CrossRef]
66. Li, M.; Chen, T.; Gooding, J.J.; Liu, J. Review of Carbon and Graphene Quantum Dots for Sensing. *ACS Sens.* **2019**, *4*, 1732–1748. [CrossRef]
67. Franco, C.A.; Candela, C.H.; Gallego, J.; Marin, J.; Patiño, L.E.; Ospina, N.; Patiño, E.; Molano, M.; Villamil, F.; Bernal, K.M.; et al. Easy and Rapid Synthesis of Carbon Quantum Dots from Mortiño (Vaccinium Meridionale Swartz) Extract for Use as Green Tracers in the Oil and Gas Industry: Lab-to-Field Trial Development in Colombia. *Ind. Eng. Chem. Res.* **2020**, *59*, 11359–11369. [CrossRef]
68. Franco, C.A.; Zapata, K.; Paramo, L.; Garzón, P.; Ramírez, D.; Jaramillo, D.; Cortes, F.B. Development of Novel Nanodetectors in Drilling Fluids To Identify the Contribution of Different Producing Zones in Naturally Fractured Carbonate Reservoirs: From the Laboratory to Field-Level Implementation. *Energy Fuels* **2023**, *37*, 7746–7759. [CrossRef]
69. Lim, S.Y.; Shen, W.; Gao, Z. Carbon quantum dots and their applications. *Chem. Soc. Rev.* **2015**, *44*, 362–381. [CrossRef] [PubMed]
70. Wang, R.; Lu, K.-Q.; Tang, Z.-R.; Xu, Y.-J. Recent progress in carbon quantum dots: Synthesis, properties and applications in photocatalysis. *J. Mater. Chem. A* **2017**, *5*, 3717–3734. [CrossRef]
71. El-Shabasy, R.M.; Farouk Elsadek, M.; Mohamed Ahmed, B.; Fawzy Farahat, M.; Mosleh, K.N.; Taher, M.M. Recent developments in carbon quantum dots: Properties, fabrication techniques, and bio-applications. *Processes* **2021**, *9*, 388. [CrossRef]
72. Ding, X.; Niu, Y.; Zhang, G.; Xu, Y.; Li, J. Electrochemistry in Carbon-based Quantum Dots. *Chem. Asian J.* **2020**, *15*, 1214–1224. [CrossRef] [PubMed]
73. Rao, V.N.; Reddy, N.L.; Kumari, M.M.; Cheralathan, K.K.; Ravi, P.; Sathish, M.; Neppolian, B.; Reddy, K.R.; Shetti, N.P.; Prathap, P.; et al. Sustainable hydrogen production for the greener environment by quantum dots-based efficient photocatalysts: A review. *J. Environ. Manag.* **2019**, *248*, 109246. [CrossRef]
74. Wang, Y.; Hu, A. Carbon quantum dots: Synthesis, properties and applications. *J. Mater. Chem. C* **2014**, *2*, 6921. [CrossRef]
75. Wang, Z.; Hu, T.; Liang, R.; Wei, M. Application of Zero-Dimensional Nanomaterials in Biosensing. *Front. Chem.* **2020**, *8*, 320. [CrossRef] [PubMed]
76. Guo, B.; Yu, K.; Li, H.; Qi, R.; Zhang, Y.; Song, H.; Tang, Z.; Zhu, Z.; Chen, M. Coral-Shaped MoS_2 Decorated with Graphene Quantum Dots Performing as a Highly Active Electrocatalyst for Hydrogen Evolution Reaction. *ACS Appl. Mater. Interfaces* **2017**, *9*, 3653–3660. [CrossRef]
77. Guo, J.; Zhu, H.; Sun, Y.; Tang, L.; Zhang, X. Doping MoS_2 with Graphene Quantum Dots: Structural and Electrical Engineering towards Enhanced Electrochemical Hydrogen Evolution. *Electrochim. Acta* **2016**, *211*, 603–610. [CrossRef]
78. Lv, J.-J.; Zhao, J.; Fang, H.; Jiang, L.-P.; Li, L.-L.; Ma, J.; Zhu, J.-J. Incorporating Nitrogen-Doped Graphene Quantum Dots and Ni_3S_2 Nanosheets: A Synergistic Electrocatalyst with Highly Enhanced Activity for Overall Water Splitting. *Small* **2017**, *13*, 1700264. [CrossRef] [PubMed]
79. Wang, X.; Yuan, W.; Yu, Y.; Li, C.M. Synthesis of Cobalt Phosphide Nanoparticles Supported on Pristine Graphene by Dynamically Self-Assembled Graphene Quantum Dots for Hydrogen Evolution. *ChemSusChem* **2017**, *10*, 1014–1021. [CrossRef]
80. Manikandan, V.; Lee, N.Y. Green synthesis of carbon quantum dots and their environmental applications. *Environ. Res.* **2022**, *212*, 113283. [CrossRef]
81. Cao, M.; Li, Y.; Song, X.; Chen, Y.; Sun, L.; Shi, X.; Dai, C.; Yuan, B. Carbon dots nanofluid: Reducing injection pressure in unconventional reservoir by regulating oil/water/rock interfacial properties. *Fuel* **2023**, *352*, 129046. [CrossRef]
82. Razavifar, M.; Khoshsima, A.; Riazi, M.; Sheng, J.J.; Esmaeilnezhad, E. Recent developments, challenges, and prospects of carbon dots (CDs) for fluid flow investigation in porous media. *Pet. Res.* **2024**, *9*, 553–564. [CrossRef]
83. Powell, K.C.; Damitz, R.; Chauhan, A. Relating emulsion stability to interfacial properties for pharmaceutical emulsions stabilized by Pluronic F68 surfactant. *Int. J. Pharm.* **2017**, *521*, 8–18. [CrossRef]
84. Ettefaghi, E.-o.-l.; Rashidi, A.; Ghobadian, B.; Najafi, G.; Khoshtaghaza, M.H.; Sidik, N.A.C.; Yadegari, A.; Xian, H.W. Experimental investigation of conduction and convection heat transfer properties of a novel nanofluid based on carbon quantum dots. *Int. Commun. Heat Mass Transf.* **2018**, *90*, 85–92. [CrossRef]
85. Chun, A.H.C.; Martin, A.N. Measurement of Hydrophile-Lipophile Balance of Surface-Active Agents. *J. Pharm. Sci.* **1961**, *50*, 732–736. [CrossRef] [PubMed]
86. Speight, J. Petroleum Asphaltenes—Part 1: Asphaltenes, resins and the structure of petroleum. *Oil Gas Sci. Technol.* **2004**, *59*, 467–477. [CrossRef]
87. *ASTM D6560*; Standard Test Method for Determination of Asphaltenes (Heptane Insolubles) in Crude Petroleum and Petroleum Products. ASTM International: West Conshohocken, PA, USA, 2000.

88. Iatroscan. IP 469: Determination of Saturated, Aromatic and Polar Compounds in Petroleum Products by Thin Layer Chromatography and Flame Ionization Detection. 2001. Available online: https://www.energyinst.org/technical/publications/topics/ip-test-methods/ip-469-determination-of-saturated,-aromatic-and-polar-compounds-in-petroleum-products-by-thin-layer-chromatography-and-flame-ionization-detection (accessed on 1 January 2025).
89. Cardona, L.; Medina, O.E.; Céspedes, S.; Lopera, S.H.; Cortés, F.B.; Franco, C.A. Effect of Steam Quality on Extra-Heavy Crude Oil Upgrading and Oil Recovery Assisted with PdO and NiO-Functionalized Al_2O_3 Nanoparticles. *Processes* **2021**, *9*, 1009. [CrossRef]
90. *ASTM-D7042*; Standard Test Method for Dynamic Viscosity and Density of Liquids by Stabinger Viscometer (and the Calculation of Kinematic Viscosity). ASTM International: West Conshohocken, PA, USA, 2010.
91. Ashoori, S.; Sharifi, M.; Masoumi, M.; Mohammad Salehi, M. The relationship between SARA fractions and crude oil stability. *Egypt. J. Pet.* **2017**, *26*, 209–213. [CrossRef]
92. Asomaning, S. Test Methods for Determining Asphaltene Stability in Crude Oils. *Pet. Sci. Technol.* **2003**, *21*, 581–590. [CrossRef]
93. Xiong, R.; Guo, J.; Kiyingi, W.; Feng, H.; Sun, T.; Yang, X.; Li, Q. Method for Judging the Stability of Asphaltenes in Crude Oil. *ACS Omega* **2020**, *5*, 21420–21427. [CrossRef]
94. Chen, R.; Zhang, Z.; Feng, C.; Hu, K.; Li, M.; Li, Y.; Shimizu, K.; Chen, N.; Sugiura, N. Application of simplex-centroid mixture design in developing and optimizing ceramic adsorbent for As(V) removal from water solution. *Microporous Mesoporous Mater.* **2010**, *131*, 115–121. [CrossRef]
95. Sapalidis, A.A. Porous Polyvinyl Alcohol Membranes: Preparation Methods and Applications. *Symmetry* **2020**, *12*, 960. [CrossRef]
96. Socrates, G. *Infrared and Raman Characteristic Group Frequencies: Tables and Charts*; John Wiley & Sons: Hoboken, NJ, USA, 2001.
97. McIntosh, I.M.; Nichols, A.R.L.; Tani, K.; Llewellin, E.W. Accounting for the species-dependence of the 3500 cm^{-1} H2Ot infrared molar absorptivity coefficient: Implications for hydrated volcanic glasses. *Am. Miner.* **2017**, *102*, 1677–1689. [CrossRef]
98. Gallego Arias, J.F. Increase in the Oil Recovery Factor through the Injection of Nano-Chemicals Dispersed in Gas. In Proceedings of the SPE Annual Technical Conference and Exhibition, Houston, TX, USA, 3–5 October 2022.
99. Subramanian, D.; May, N.; Firoozabadi, A. Functional Molecules and the Stability of Water-in-Crude Oil Emulsions. *Energy Fuels* **2017**, *31*, 8967–8977. [CrossRef]
100. Medina, O.E.; Gallego, J.; Restrepo, L.G.; Cortés, F.B.; Franco, C.A. Influence of the Ce^{4+}/Ce^{3+} Redox-couple on the cyclic regeneration for adsorptive and catalytic performance of NiO-PdO/$CeO_{2\pm\delta}$ nanoparticles for n-C7 asphaltene steam gasification. *Nanomaterials* **2019**, *9*, 734. [CrossRef] [PubMed]
101. Andersen, S.I.; Speight, J.G. Thermodynamic models for asphaltene solubility and precipitation. *J. Pet. Sci. Eng.* **1999**, *22*, 53–66. [CrossRef]
102. Nguele, R.; Mbouopda Poupi, A.B.; Anombogo, G.A.M.; Alade, O.S.; Saibi, H. Influence of asphaltene structural parameters on solubility. *Fuel* **2022**, *311*, 122559. [CrossRef]
103. Binks, B.P.; Lumsdon, S.O. Transitional Phase Inversion of Solid-Stabilized Emulsions Using Particle Mixtures. *Langmuir* **2000**, *16*, 3748–3756. [CrossRef]
104. Khivantsev, K.; Jaegers, N.R.; Kovarik, L.; Derewinski, M.A.; Kwak, J.-H.; Szanyi, J. On the Nature of Extra-Framework Aluminum Species and Improved Catalytic Properties in Steamed Zeolites. *Molecules* **2022**, *27*, 2352. [CrossRef]
105. Gardelle, B.; Duquesne, S.; Vandereecken, P.; Bourbigot, S. Resistance to fire of silicone-based coatings: Fire protection of steel against cellulosic fire. *J. Fire Sci.* **2014**, *32*, 374–387. [CrossRef]
106. Shao, H.; Zhou, Y.; Qi, J.; Hu, P.; He, J. Characterization of Fe_3O_4/γ-Fe_2O_3@ SiO_2 Core-Shell Structure Composite Magnetic Fluid by Microemulsion Method. *J. Supercond. Nov. Magn.* **2019**, *32*, 247–252. [CrossRef]
107. Pham, X.N.; Nguyen, T.P.; Pham, T.N.; Tran, T.T.N.; Tran, T.V.T. Synthesis and characterization of chitosan-coated magnetite nanoparticles and their application in curcumin drug delivery. *Adv. Nat. Sci. Nanosci. Nanotechnol.* **2016**, *7*, 045010. [CrossRef]
108. Alvarado, J.G.; Delgado-Linares, J.G.; Forgiarini, A.M.; Salager, J.-L. Breaking of Water-in-Crude Oil Emulsions. 8. Demulsifier Performance at Optimum Formulation Is Significantly Improved by a Small Aromatic Content of the Oil. *Energy Fuels* **2019**, *33*, 1928–1936. [CrossRef]
109. Salager, J.-L.; Forgiarini, A.M. Emulsion Stabilization, Breaking, and Inversion Depends upon Formulation: Advantage or Inconvenience in Flow Assurance. *Energy Fuels* **2012**, *26*, 4027–4033. [CrossRef]
110. Wasan, D.T. Destabilization of Water-in-Oil Emulsions. In *Emulsions—A Fundamental and Practical Approach*; Sjöblom, J., Ed.; Springer: Dordrecht, The Netherlands, 1992; pp. 283–295.
111. Hippmann, S.; Ahmed, S.S.; Fröhlich, P.; Bertau, M. Demulsification of water/crude oil emulsion using natural rock Alginite. *Colloids Surf. A Physicochem. Eng. Asp.* **2018**, *553*, 71–79. [CrossRef]
112. Razi, M.; Rahimpour, M.R.; Jahanmiri, A.; Azad, F. Effect of a Different Formulation of Demulsifiers on the Efficiency of Chemical Demulsification of Heavy Crude Oil. *J. Chem. Eng. Data* **2011**, *56*, 2936–2945. [CrossRef]
113. Becker, J.R. *Crude Oil Waxes, Emulsions, and Asphaltenes*; Pennwell Books: Tulsa, OK, USA, 1997; ISBN 978-0-87814-737-3.
114. Mohyaldinn, M.E.; Rammudo, L.; Ayoub, M. Experimental investigation of polyvinylpyrrolidone for application as a demulsifier for water-in-oil emulsion. *Open Pet. Eng. J.* **2017**, *10*, 263–275. [CrossRef]

115. Avranas, A.; Stalidis, G.; Ritzoulis, G. Demulsification rate and zeta potential of O/W emulsions. *Colloid Polym. Sci.* **1988**, *266*, 937–940. [CrossRef]
116. Mikula, R.J.; Munoz, V.A. Characterization of Demulsifiers. In *Surfactants: Fundamentals and Applications in the Petroleum Industry*; Schramm, L.L., Ed.; Cambridge University Press: Cambridge, UK, 2000; pp. 51–78.
117. Feng, X.-J.; Tang, Y.-J.; Yang, Y.; Wang, G.; Mei, P.; Lai, L. Relationship Between the Dynamic Interfacial Activity and Demulsification Performance of Hyperbranched Poly(amido amine) Polyethers. *Colloids Surf. A Physicochem. Eng. Asp.* **2022**, *633*, 127869. [CrossRef]
118. Yang, H.-L.; Bai, L.-F.; Geng, Z.-R.; Chen, H.; Xu, L.-T.; Xie, Y.-C.; Wang, D.-J.; Gu, H.-W.; Wang, X.-M. Carbon quantum dots: Preparation, optical properties, and biomedical applications. *Mater. Today Adv.* **2023**, *18*, 100376. [CrossRef]
119. Issaka, S.A.; Nour, A.H.; Yunus, R.b.M. Review on the Fundamental Aspects of Petroleum Oil Emulsions and Techniques of Demulsification. *J. Pet. Environ. Biotechnol.* **2015**, *6*, 1–15. [CrossRef]
120. Abdulrahman, I.; Máša, V.; Teng, S.Y. Process intensification in the oil and gas industry: A technological framework. *Chem. Eng. Process. Process Intensif.* **2021**, *159*, 108208. [CrossRef]
121. Kim, Y.C.; Yoon, H. Exploitation of acetic acid for calcite dissolution in small-capacity desalination plants. *Desalination* **2021**, *516*, 115227. [CrossRef]
122. Kokal, S. Crude-Oil Emulsions: A State-Of-The-Art Review. *SPE Prod. Facil.* **2005**, *20*, 5–13. [CrossRef]
123. Fan, Y.; Simon, S.; Sjöblom, J. Chemical Destabilization of Crude Oil Emulsions: Effect of Nonionic Surfactants as Emulsion Inhibitors. *Energy Fuels* **2009**, *23*, 4575–4583. [CrossRef]
124. Sousa, A.M.; Pereira, M.J.; Matos, H.A. Oil-in-water and water-in-oil emulsions formation and demulsification. *J. Pet. Sci. Eng.* **2022**, *210*, 110041. [CrossRef]

Disclaimer/Publisher's Note: The statements, opinions and data contained in all publications are solely those of the individual author(s) and contributor(s) and not of MDPI and/or the editor(s). MDPI and/or the editor(s) disclaim responsibility for any injury to people or property resulting from any ideas, methods, instructions or products referred to in the content.